Ocean Sci. Discuss., 12, 769–822, 2015
www.ocean-sci-discuss.net/12/769/2015/
doi:10.5194/osd-12-769-2015

Ocean Science
Discussions
Open Access

Distribution of intermediate water masses in the subtropical northeast Atlantic

I. Bashmachnikov[1,2], **Â. Nascimento**[1], **F. Neves**[1], **and T. Menezes**[1]

[1]MARE – Marine and Environmental Sciences Centre, Faculdade de Ciências, Universidade de Lisboa, Campo Grande, 1749-016 Lisboa, Portugal
[2]Departamento de Engenharia Geográfica, Geofísica e Energia (DEGGE), Faculdade de Ciências, Universidade de Lisboa, Campo Grande, 1749-016 Lisboa, Portugal

Received: 2 April 2015 – Accepted: 27 April 2015 – Published: 21 May 2015

Correspondence to: I. Bashmachnikov (igorb@fc.ul.pt)

Published by Copernicus Publications on behalf of the European Geosciences Union.

Abstract

This work presents the quantitative study of climatological distributions of mid-depth Source Water Types in the NE Atlantic by the Optimum Multiparameter analysis (OMP), merging a number of regional results from particular synoptic sections. The cores of the Mediterranean Water (MW), the modified Antarctic Intermediate Water (mAAIW) and the Subarctic Intermediate Water (SAIW) are detected and spatial variations of their depth/density are obtained: as expected, spreading of the source water types is predominantly isopycnic and follows the major mid-depth circulation patterns. In some areas the turbulent transport should also be considered.

The MW in the Atlantic spreads as 3 cores of different density: the upper MW core (northwest of the first transition line between 28° W, 35° N and 14° W, 44° N) is found in the neutral density range of 27.65–27.70 kg m^{-3} and depths of 900–1000 m; the main MW core (northwest of the second transition line between 35° W, 28° N and 10° W, 37° N) has neutral density around 27.75 kg m^{-3} and is found at 1000–1100 m; the lower MW core (southeast of the second transition) has neutral density around 27.80 kg m^{-3} and is found at 1250–1350 m. The upper MW core has comparatively low MW contents (below 30 %) and is speculated to be transported by the mean flow from the northern Iberian Peninsula and the Bay of Biscay to the northern Azores. The main MW core contains the most of the MW. It primarily originates from the MUC between Cape St. Vincent and Estremadura Promontory, where the strongest local decrease of the topographic β-effect is detected and is transported west by a flow at around 39° N. The lower MW core originates in the Gulf of Cadiz and is translated southwestwards by dominating flows.

The SAIW (the core between 27.70 and 27.75 kg m^{-3}) is found to spread south along both slopes of the MAR. The SAIW east of the MAR mixes with the upper and the main MW cores and re-circulates in a cyclonic gyre at 15–25° W and 34–39° N as far south as the Azores Current.

OSD

12, 769–822, 2015

The northernmost spreading limit of the mAAIW (the core between 27.60 and 27.65 kg m^{-3}) is at 25–29° N, but its influence reaches 32° N east and west of the Canary Islands. Its maximum concentration is found south of the Canaries, from where the mAAIW is transported westwards, parallel to the westward transport of the deep fraction of the MW.

1 Introduction

Thermohaline properties of deep oceanic waters are formed in the upper mixed layer under the effects of radiation balance and ocean–atmosphere heat/fresh water exchange. The near-surface water can be subducted to deeper ocean layers as a result of downwards Ekman pumping or deep winter convection. The first mechanism (the ventilated thermocline) is only active in the area of the negative wind stress curl (Pedlosky, 1998). The most favorable subduction conditions are formed in the regions of a substantial vertical tilt of near-surface isopycnals that allow isopycnic downwards motion. In the NE Atlantic those conditions are verified along the frontal zones of the branches of the North Atlantic Current (Tomczak and Godfrey, 2003; Cianca et al., 2009), where various modes of the North Atlantic Central Water are formed. The subduction is the most efficient in winter, when the internal water structure is not sheltered by the seasonal thermocline. The deep convection is a results of the gravitational instability and is mostly active in weakly stratified polar waters in winter due to intensive heat loss and salinification in the course of ice formation (van Aken, 2000a).

Below the seasonal pycnocline, having lost connection with the ocean surface, water changes its thermohaline properties mainly as a result of mixing with waters with different properties. When a subduction/convection process is regular, large collections of water parcels with a common formation history spread across the ocean, called water masses or source water types (Tomczak and Large, 1989). Formed as a result of local vertical mixing, the cores of the source water types form local minima of potential vorticity.

OSD
12, 769–822, 2015

In this study qualitative estimates of water mass properties are obtained to refine depths of their cores and the limits of their spreading across the northeast Atlantic, between 25–45° N and 5–35° W.

Below we present a brief overview of water masses in the subtropical NE Atlantic.

1.1 Upper water masses: the NACW

The principal water mass of the North Atlantic main thermocline, the North Atlantic Central Water (NACW), is composed from various fractions or modes, formed in different areas of the North Atlantic. The NACW is characterized by a nearly straight line in T-S diagrams, connecting two T-S points: west of the Mid Atlantic Ridge (the Western NACW – WNACW) – the deep point is (7.0–8.5 °C; 35.0–35.1) and the near-surface point is (18.0–19.0 °C; 36.4–36.6); east of the Mid Atlantic Ridge (the Eastern NACW – ENACW) – the deep point the deep point is (8.5–9.5 °C; 35.2–35.3) and the near-surface point is (18.0–19.0 °C; 36.5–36.7) (Harvey and Arhan, 1988; Pollard et al., 1996). The WNACW consists of: 13 °C mode water (with temperature around 13 °C) formed at the frontal zone of the North Atlantic Current northwest of the Azores between 45–50° N (McCartney, 1982; Paillet and Arhan, 1996b), and 18 °C mode water formed at the Gulf Stream frontal zone (Harvey and Arhan, 1988). Various modes of the WNACW are advected eastward or southeastward and, crossing the Mid Atlantic Ridge (MAR), enter in the region of interest (Pollard and Pu, 1985; Harvey and Arhan, 1988). The ENACW occupies the same depth range as the WNACW, but for the same temperatures the former is on average 0.1 more saline (van Aken, 2001). The ENAWC consists of: the 11–12 °C polar ENACW ($ENACW_p$) formed by subduction at a sharply deepening winter pycnocline at the southwestern edge of the Bay of Biscay at 40–50° N and 20° W, and the 18 °C tropical ENACW ($ENACW_t$) formed in a westward recirculation of the Azores Current near the Iberian Peninsula (Pérez et al., 1993; Pollard et al., 1996). There are indications that some of the 18 °C water is also formed near Madeira Island – the Madeira Mode Water (Siedler et al., 1987; Pingree et al.,

OSD
12, 769–822, 2015

1999; New et al., 2001). The lowest fraction of the NACW represents a mixture of the lower WNACW or $ENACW_p$ with deeper water masses.

In the study region, most of the upper NACW between 200–400 m is represented by the upper WNACW, transported in the area by southeastwards flows, and the $ENACW_t$ is observed only over a very limited area close to its formation region (Pollard and Pu, 1985; Paillet and Arhan, 1996a, b). The main source of the deeper NACW, as far east as the MAR and north of the Azores Current, is the $ENACW_p$ (Pérez et al., 1993; Pallet and Arhan, 1996a, b; van Aken, 2001).

The upper NACW in the southwestern part of the study region is affected by the subtropical Mode Water (StrMW). The StrMW is characterized by elevated temperature (over 18 °C) and salinity (36.7) and comparatively low oxygen and high nutrient contents (Kremeur et al., 2009). The StrMW is formed south to the Gulf Stream as a result of an intense surface heat loss during winter storms (Maze and Marshall, 2011).

In T-S diagrams the NACW lines (either the WNACW or the ENACW) are slightly curved and can be better approximated with two sections of a broken line. To account for this feature in water mass analysis, an additional water type (H) is introduced with temperature 12.0–12.20 and salinity 35.6–35.7 (Pérez et al., 1998; Alvaréz et al., 2004; Barbero et al., 2010). It is placed at the maximum curvature of the T-S line, the junction between the upper and the lower NACW, and in the study region is found at about 500 m.

1.2 Intermediate water masses: the MW, the SAIW and the AAIW

At the intermediate water levels (700–1500 m depth) a mixture of the Mediterranean Water (MW), the Subarctic Intermediate Water (SIAW) and the Antarctic Intermediate Water (AAIW) is observed.

The SAIW is a relatively cold and fresh water mass with high oxygen contents, formed west of the MAR at the northern branch of the North Atlantic Current (50–54° N). A part of the SAIW (with temperature 4–7 °C) is advected northwest between 45–55° N, with the northern branch the North Atlantic Current. Another part of the SAIW

OSD
12, 769–822, 2015

(with temperature 9–10 °C) spreads southeast, along both sides of the MAR, down to 40–45° N, gradually mixing with the NACW (McCartney and Talley, 1982; Harvey and Arhan, 1988; Arhan, 1990). North of the Azores the mixed SAIW is observed at 700–1000 m (Tsuchiya, 1989; Arhan, 1990). Some traces of the SAIW are found to spread east to 20–25° W (Arhan, 1990; Arhan et al., 1994) or to 10° W (McCartney and Talley, 1982). The SAIW forms a front with the main body of the Mediterranean Water from the eastern tip of the Azores rise to the Bay of Biscay (Arhan et al., 1994).

The AAIW found in the Atlantic is formed at the Antarctic Polar Front and the neighboring Scotia Sea (Schmitz, 1996; Tomczak and Godfrey, 2003). The AAIW spreads north with the Malvinas Current and further, with the currents of the South Atlantic subtropical gyre and the equatorial current system, it enters the North Atlantic. In the North Atlantic the AAIW is observed between 700 and 900 m and is characterized by temperature over 3 °C, salinity minimum of 34.45–34.50, oxygen minimum and silicate maximum (Schmitz, 1996). The characteristics are quite different from the ones in the generation region (temperature of 2.2 °C and salinity of 33.8), and in the North Atlantic it is called the modified AAIW (mAAIW, sometimes also called the AA – Pérez et al., 1998, 2001; Alvaréz et al., 2004). In the NE Atlatic the mAAIW is traced as a salinity minimum up to 25–26° N (Tsuchiya et al., 1992), but using nutrient anomalies it can be traced along the African coast up to 30–32° N (Alvaréz et al., 2004; Machin et al., 2006). Some traces of the mAAIW are detected as far north as the Gulf of Cadiz (Louarn and Morin, 2011). Another portion of the mAAIW spreads along the American continental slope with the Caribbean Current, the Gulf Stream and the North Atlantic Current, entering the study region from the northwest. This substantially diluted mAAIW (temperature of 6–11 °C and salinity less than 35.5) can be detected just above the MW, at 500–800 m depth, as a silica maximum and a weak salinity-oxygen minimum (Tsuchiya et al., 1992; Arhan et al., 1994).

The MW is formed from the outflow of the anomalously saline and warm Mediterranean Sea water in the Atlantic. The MW also has low oxygen and nutrient content. Over a significant part of the NE Atlantic the MW influences the water column from

OSD
12, 769–822, 2015

700 to 1500 m, although some weak MW influence is detected down to 3000 m depth (Tsuchiya et al., 1992; Arhan et al., 1994). From the Gibraltar Strait the MW spreads as the Mediterranean Undercurrent (MUC), trapped by the continental slope of the Iberian Peninsula. In the Gulf of Cadiz the MUC deepens from 100 m (near the Strait of Gibraltar) to its neutral buoyancy level at 1200–1300 m (Price et al., 1993). The sinking is accompanied by mixing of the Mediterranean Water with the NACW and the upper North Atlantic Deep Water. The entrainment of the ambient water masses increases the MUC transport by 2/3 of its initial value, and the original MW properties are strongly modified (Price et al., 1993; van Aken, 2000b; Barbosa Aguiar et al., 2014). The major part of thus modified MW leaves the continental slope south of Estremadura Promontory (39° N) to spread west and southwest, but lighter fractions of the MW follow the continental margin of the Bay of Biscay and join the North Atlantic Current northwest of the Irish continental slope (Daniault et al., 1994; Mazé et al., 1997; Iorga and Lozier, 1999a). The main fraction of the MW spreads to the Azores rise at 800–1000 m, while the lower fraction of the MW preferably spreads south of the Azores Current at 1000–1200 m (Harvey and Arhan, 1988; Iorga and Lozier, 1999a). The main MW is considered to be the "pure" MW, while the lower fraction of the MW is, presumably, its mixture with the North Atlantic Deep Water (van Aken, 2000b).

1.3 Deep water masses: the LSW and the NADW

The Labrador Sea Water (LSW) is formed by deep convection in the Labrador Sea. The LSW is cold and fresh and has higher oxygen content. The LSW penetrates the NE Atlantic crossing the MAR through Charlie Gibbs Fracture zone (Talley and McCartney, 1982; Straneo et al., 2003). The major part of the LSW spreads south along the eastern slope of the MAR at the speed of order of 1 cm s^{-1}, skirting the eastern slope of the Azores rise at 1200–2500 m (Harvey and Arhan, 1988; Paillet et al., 1998; Bower et al., 2002a). A temperature/salinity front, which separates the LSW from the MW, is approximately aligned with that between the MW and the SAIW (Paillet et al., 1998).

OSD
12, 769–822, 2015

The influence of the LSW decreases south and southwest; no LSW is expected in the southeastern part of the study region.

The North Atlantic Deep Water (NADW) is detected in the depth range between 1000 and 4000 m over the whole Atlantic. There are several fractions of the NADW. The main ones are the upper NADW, or the Iceland–Scotland Overflow Water (ISOW), and the lower NADW, or the Low Deep Water (LDW). The core of the cold oxygenated NADW is formed as a result of deep convection in the Greenland Sea. It spreads south mainly through Denmark Strait west of Iceland, but also over the Faeroe–Iceland and the Faeroe–Scotland ridges east of Iceland. The NADW south east of Island strongly mixes with the water of the North Atlantic Current over relatively shallow Faeroe–Iceland and Faeroe–Scotland sills, forming the upper NADW (Tsuchiya et al., 1992). It is slightly colder and more saline than the LSW and in the subtropical NE Atlantic it is observed from 2500–3000 m below (Harvey and Arhan, 1988). The upper NADW mostly enters the study region from the north, but also from the west and southwest (Schmitz, 1996; Brix and Gerdes, 2003).

The NADW west of Iceland enters the western North Atlantic basin and mixes with the LSW, forming the lower NADW (Harvey and Arhan, 1988). Some of the lower NADW enters the NE Atlantic through the Charlie Gibbs Fracture zone, but most of the lower NADW is thought to enter NE Atlantic basin at around 10° N and to spread north together with the Antarctic Bottom Water (AABW) below 3500 m. The AABW is formed at the Antarctic continental slope (Orsi et al., 2001). Diapycnal mixing with the AABW modifies the deeper fraction of the lower NADW (van Aken, 2000a).

2 Data and methods

2.1 The data-sets

Temperature and salinity, the principal parameters for water mass identification in the OMP analysis, were downloaded from the regional MEDTRANS climatology (http:

OSD
12, 769–822, 2015

//co.fc.ul.pt/pt/dados-medtrans). In the subtropical NE Atlantic, the MEDTRANS climatology has advantage over other climatologies (including the World Ocean Atlas 2013) in the representation of temperature and salinity distributions in the areas with sharp horizontal gradients of the characteristics: in particular, the MW Undercurrent (Bashmachnikov et al., 2015a). Nutrients (nitrate, phosphate and silicate) and oxygen are not available in the MEDTRANS climatology and were downloaded from the World Ocean Atlas database (WOA13, http://www.nodc.noaa.gov/OC5/woa13). Both MEDTRANS and WOA13 climatologies are based on Barnes' Optimum Interpolation analysis (Barnes, 1964). The hydrological and nutrient data are gridded to the regular grid with 30 km horizontal resolution and 25 m vertical resolution. Neutral density surfaces, a generalization of isopycnic surfaces referenced to a fixed depth, are computed from the temperature-salinity distributions (McDougall, 1987; Jackett and McDougall, 1997).

The deep ocean circulation in the turbulent ocean presents a problem, hindered by internal wave and eddy activity, and has been studied in the subtropical NE Atlantic with insufficient detail (Bower et al., 2002a; Ollitrault and Colin de Verdière, 2014; Carracedo et al., 2014). In this study the pathways of water transport, derived from the obtained spatial variations of contents of the source water types, are compared to the circulation patterns, derived from RAFOS and ARGO floats. The RAFOS float data are downloaded from the WOCE Subsurface Float Data Assembly Center (http://wfdac.whoi.edu/). The data set of 353 floats used covers depths interval from 400 to 1700 m and the period from 1982 to 2002. The typical sampling period is a day or less and the overall duration of the observations is 6700 float-months. The ARGO float data-set is obtained from the Coriolis operational data center (ftp://ftp.ifremer.fr). The data set of 242 ARGO floats used covers the same depth range and the period from 1999 to 2013. The typical sampling period is 10–15 days and the overall duration of the observations is 6560 float-months. Since mesoscale eddies often have velocities different from those of the ambient flow (Morel, 1995), the parts of the trajectories within eddies are blanked to avoid the bias. Difference in the sampling periods (rotations in

OSD
12, 769–822, 2015

mesoscale eddies have characteristic periods of 3–10 days and can be registered in RAFOS, but not in ARGO data) and the observed water properties (the majority of the RAFOS floats register only along-track temperature and pressure, while ARGO floats supply vertical temperature-salinity profiles from 2000 m to the sea-surface at the end of every sampling period) leads to different eddy identification algorithms in each of the data-sets. For a RAFOS float, eddies are detected as the parts of the trajectory, where at least 2 complete rotations are registered within a 20 day interval. Most of eddies detected at mid-depths has been previously identified as Mediterranean water eddies (meddies – Richardson et al., 2000; Ambar et al., 2001). Meddies are the strongest mid-depth eddies in the subtropical NE Atlantic and it is important to filter their effect in the data-set. ARGO profiling floats allow to securely remove meddies, identified as strong salinity anomaly over 0.2 more than 200 m thick within 500–1500 m depth interval (Richardson et al., 1991), referenced to the MEDTRANS climatology.

The filtered trajectories are collected for different referenced depths of interest within ±500 m depth interval. In each of the sets, the Lagrangian floats velocities are computed and are reduced from the float depth to the reference depth using geostrophic relation:

$$\frac{\partial V}{\partial z} = \frac{g}{f\,\overline{\rho}}\,(\boldsymbol{k}\cdot\nabla)\,\rho,$$

where V is the Lagrangian horizontal velocity, g is the acceleration of gravity, f is the Coriolis parameter, ρ is the water density (obtained from the MEDTRANS climatology), $\overline{\rho}$ is the characteristic value of ρ. The Eulerian mean velocities and the associated errors are further computed in each of the $1^\circ \times 1^\circ$ squares. To account for the difference in the float sampling periods, the Lagrangian velocities in the means are weighted with the respective sampling periods (Lavender et al., 2005). The velocity errors are computed as: $v_{\mathrm{err}} = z_{95}\mathrm{SD}/\sqrt{n}$, where n is the number of the data-point, SD is the SDs of meridional or zonal components of the flow and z_{95} is 95 % confidence interval of the Student's t distribution. The outliers in the Eulerian velocity fields are smoothed out by the discrete cosine transform – penalized least

OSD
12, 769–822, 2015

square method (Garcia, 2011). This filtering is not applied at the steep sloping topography, where a rapid variation of current velocity (a bottom trapped flow) is expected. The bottom slopes are identified from the GEBCO $1' \times 1'$ bathymetry data-set (http://www.gebco.net/data_and_products/gridded_bathymetry_data/).

2.2 The Optimum Multiparameter analysis set-up

The quantitative estimate of relative contributions of the main source water types in the study region is obtained with the Optimum Multiparameter (OMP) analysis (Tomczak, 1981; Mackas et al., 1987; Tomczak and Large, 1989). The OMP analysis assumes that, below the upper mixed layer, all water characteristics vary only as a result of mixing between the interacting source water types, and that the mixing intensities of different water characteristics are the same. Contributions from the predefined source water types in each of the data-points is determined by inversing the system of linear equations, where each of the observed water properties in a data-point is decomposed into a combination of the known source water types' characteristics multiplied by their unknown contributions. The classical OMP analysis considers all parameters as passive tracers, and the maximum number of the simultaneously resolved source water types is limited by the number of water characteristics measured in-situ. The method has been successfully applied to study of spatially limited regional mixing and circulation patterns (e.g. Klein and Tomczak, 1994). Applied to ocean-basin scales, the non-conservative variation of nutrients due to biochemical processes in the water column (the water mass aging) has to be taken into account. The unknown rates of remineralisation of nutrients due to oxidation have to be incorporated in the equations as additional variables (Karstensen and Tomczak, 1997; Poole and Tomczak, 1999). An additional assumption of the equal rate of remineralisation of all the nutrients and of the proportional decrease of oxygen in the process of oxidation of the subducted detritus allows to reduce the number of additional biochemical unknowns to one (Karstensen and Tomczak, 1997; Poole and Tomczak, 1999). Due to the predominantly biological origin of the detritus in the open ocean, the rates of nitrogen, oxygen, etc. variations

OSD
12, 769–822, 2015

due to remineralisation can be converted into phosphate variation using their stochiometric ratios in phytoplankton (Karstensen and Tomczak, 1997). The latter are known as Redfield ratios (Redfield et al., 1963). This methodology, known as the Extended OMP analysis, is applied in this paper.

The Extended OMP code is developed by J. Karstensen and M. Tomczak (http://omp.geomar.de). The water characteristics used are: potential temperature (θ), salinity (S), oxygen (O_2), nitrate (NO_3^-), phosphate (PO_4^{3-}) and silicate ($Si(OH)_4$, further labeled as Si), and the system of equations is:

$$
\begin{aligned}
&x_1\theta_1 + x_2\theta_2 + x_3\theta_3 + x_4\theta_4 + x_5\theta_5 = \theta_{\mathrm{obs}} + R_\theta \\
&x_1 S_1 + x_2 S_2 + x_3 S_3 + x_4 S_4 + x_5 S_5 = S_{\mathrm{obs}} + R_S \\
&x_1 \mathrm{PO}_{4,1} + x_2 \mathrm{PO}_{4,2} + x_3 \mathrm{PO}_{4,3} + x_4 \mathrm{PO}_{4,4} + x_5 \mathrm{PO}_{4,5} + \Delta P = \mathrm{PO}_{4,\mathrm{obs}} + R_{\mathrm{PO}_4} \\
&x_1 \mathrm{NO}_{3,1} + x_2 \mathrm{NO}_{3,2} + x_3 \mathrm{NO}_{3,3} + x_4 \mathrm{NO}_{3,4} + x_5 \mathrm{NO}_{3,5} + r_{N/P}\Delta P = \mathrm{NO}_{3,\mathrm{obs}} + R_{\mathrm{NO}_3} \\
&x_1 \mathrm{O}_{2,1} + x_2 \mathrm{O}_{2,2} + x_3 \mathrm{O}_{2,3} + x_4 \mathrm{O}_{2,4} + x_5 \mathrm{O}_{2,5} - r_{\mathrm{O}/P}\Delta P = \mathrm{O}_{2,\mathrm{obs}} + R_{\mathrm{O}_2} \\
&x_1 \mathrm{Si}_1 + x_2 \mathrm{Si}_2 + x_3 \mathrm{Si}_3 + x_4 \mathrm{Si}_4 + x_5 \mathrm{Si}_5 = \mathrm{Si}_{\mathrm{obs}} + R_{\mathrm{Si}} \\
&x_1 + x_2 + x_3 + x_4 + x_5 = 1 + R_\Sigma
\end{aligned}
\tag{1}
$$

In the left-hand of the system Eq. (1), the known parameters are the characteristics of source water types ($\theta_1, \theta_2, \ldots, S_1, S_2, \ldots, \mathrm{Si}_1, \mathrm{Si}_2, \ldots, \mathrm{Si}_5$) and the biogeochemical Redfield ratios (r) of the corresponding non-conservative parameters to P. In order to make the units of different parameters commensurable, a normalization of the source water type matrix is performed (Karstensen and Tomczak, 1997). The unknown parameters are the source water type contributions $x_1, \ldots, x_5$ and the phosphate remineralisation rate ΔP. The right-hand side represents the observed values of each of the parameter ($\theta_{\mathrm{obs}}, \ldots, \mathrm{Si}_{\mathrm{obs}}$) and their respective residuals ($R_\theta, \ldots, R_{\mathrm{Si}}$). Following some of the previous studies, Si is considered a conservative tracer (van Aken, 2000a; Alvaréz et al., 2004). This is due to Si remineralisation processes are of low intensity and different from those of other nutrients, while the stochiometric ratio of Si to O_2, or to other nutrients, in phytoplankton are regional and depth dependent (van Aken, 2000a).

OSD
12, 769–822, 2015

Two additional realistic constraints are imposed on Eq. (1): the contributions from all the source water types add up to 100 % within the error $R_{\sum}$ (the last equation) and all the contributions x_1, ..., x_5 are non-negative. A non-trivial value of $R_{\sum}$ urges for an over-determined system. Therefore, the seven equations of system Eq. (1) allow simultaneous analysis of the contributions of up to five different source water types.

Results of the OMP analysis critically depend on the choice of the dominating source water types. The preliminary choice of 5 main source water types, affecting range of depths in each of the $5^{\circ} \times 5^{\circ}$ squares, is based on previous studies, described in Introduction (Tsuchiya et al., 1992; Pérez et al., 1998, 2001; Poole and Tomczak, 1999; van Aken, 2000a, b, 2001; Cabeçadas et al., 2002; Alvaréz et al., 2004; Barbero et al., 2010; Louarn and Morin, 2011). The depth limits of influence of each of the sets of upper ocean, mid-depth and deep source water types are further verified using θ-S, θ-O_2, θ-NO_3, θ-Si, etc. diagrams (see examples in Fig. 1a and b). It is clear from the plot that some STWs are nearly undistinguishable in θ-S diagrams, but are well differentiated in Si-O_2 diagrams (as the StrMW and the $NACW_u$, the SAIW and the mAAIW, the LSW and the $NADW_u$). This demonstrates the importance of the nutrients in the OMP analysis.

Since the number of source water types in the whole water column often exceeds the limit of 5, the water column is separated into 3 layers, within each of which a particular set of the source water types is used. At each particular location layer limits are obtained from local mixing triangles in θ-S, θ-O_2, θ-NO_3, θ-Si, etc. diagrams, defined as the depths of the intersections of θ-S, etc. lines between the main source water types with the observed θ-S, θ-O_2, θ-NO_3, θ-Si, etc. curves (Fig. 1).

To uniformly resolve the mid-depth source water types of interest, western and eastern fractions of the NACW are clamped together into: the upper NACW ($NACW_u$), H and the lower NACW ($NACW_l$). The StrMW is treated separately due to its comparatively vast distribution and very particular nutrient characteristics (Fig. 1b).

The extremely low values of oxygen at around 500 m depth (Fig. 1b) are a result of the influence of the Guinea Dome Water, formed near the Cape Verde Islands and ad-

OSD
12, 769–822, 2015

vected north along the African continental margin (Stramma et al., 2008). This source water type has temperature and salinity close to those in the $NACW_l$, but it is characterized by an anomalously low oxygen (70 µmol L^{-1}) and a relatively high silicate (14 µmol L^{-1}) concentrations. At the same time, the Guinea Dome Water is ignored, since its influence in the study region is low and limited to the mid-thermocline in its southernmost/southeasternmost parts. The Guinea Dome Water contents is partly incorporated in the derived contents of the mAAIW and the StrMW.

Analysis of the mixing triangles (see examples in Fig. 1a and b) results in segmentation of the water column into: the upper main thermocline layer (layer 1), the intermediate layer (layer 2), and the deep layer (layer 3). The upper boundary of layer 1 is located at the base of the winter mixed layer and the depth of its lower boundary varies from 350 and 550 m (Fig. 1c). In layer 1 the following source water types are used: the StrMW, the $NACW_u$, the H, the $NACW_l$ and the MW (the MW influences layer 1 in the Gulf of Cadiz). Layer 2 extends from the lower boundary of layer 1 to about 1200–1300 m in the northeastern part of the region and to 900–1000 m at the southwestern part of the region (Fig. 1d). The source water types of layer 2 are: the $NACW_l$, the MW, the mAAIW, the SAIW and the LSW. Layer 3 extends from the lower boundary of layer 2 to the maximum analysis depth of 2000 m. The source water types of layer 3 are: the $NACW_l$, the MW, the mAAIW, the LSW and the $NADW_u$.

The characteristics of the source water types are considered not at their source areas, but at their entry in the study region. This allows eliminating the effects of transformation of the source water types properties on their way to the study region, where they mix with the source water types not accounted for in this study. This is especially relevant for the source water types formed far away from the study region, as the mAAIW. The characteristics of the source water types (Table 1) are based on the works by Karstensen and Tomczak (1997), Pérez et al. (1998, 2001), Poole and Tomczak (1999), van Aken (2000a, b, 2001), Cabeçadas et al. (2002), Álvarez et al. (2004), Barbero et al. (2010), Louarn and Morin (2011) and Carracedo et al. (2014). In this table the mAAIW is defined as the characteristics of the AAIW near the Canary Islands

OSD
12, 769–822, 2015

(Tsuchiya et al., 1992; Pérez et al., 1998, 2001; Álvarez et al., 2004); the MW – at the southern continental slope of the Iberian Peninsula at 7° W, where the lower core of the MUC stabilizes between 800 and 1000 m depth (Baringer and Price, 1997; Bower et al., 2002b; Louarn and Morin, 2011); the LSW and the NADW – as they enter the study region from the north (Pérez et al., 1998, 2001; van Aken, 2000a, b; Álvarez et al., 2004; Barbero et al., 2010). For the SAIW and the fractions of the NACW, their properties in the place of origin are used, since they originate in the immediate vicinity of the boundaries of the study region.

In-situ observations of different water characteristics are not equally reliable and representative. Therefore, different equations of system Eq. (1) should not equally influence the OMP analysis result. Differences in instrumental accuracy of in situ measurements, in the relative dispersion of characteristics of the parameters and, for non-conservative parameters, relative accuracy of definition of their mineralization rates, are used for weighting of the equations of Eq. (1). The weights (Table 1) are adopted from the works by Tomczak and Large (1989), Álvarez et al. (2004), Barbero et al. (2010) and Louarn and Morin (2011). Silicate is given the lowest weight since its biochemical decomposition is not taken into account.

Stochiometric Redfield ratios slightly vary across ocean areas and depth levels (Anderson and Sarmiento, 1994; Dafner et al., 2003; Pérez et al., 1998, 2001). In this study $O_2 : NO_3 : PO_4 = 150 : 16 : 1$ are used as a reasonable balance between the estimates from the different parts of the Atlantic region, presented in the studies above.

2.3 The accuracy of the OMP analysis

In this section, we estimate the minimum source water type contents detectable under the selected configuration, as well as of the robustness of the results. Two different estimates of the OMP errors are considered: (i) the formal error of the fit, equal to the mass conservation residual R_Σ, and (ii) sensitivity of the results to variations of characteristics of the source water types.

OSD
12, 769–822, 2015

R_Σ over the study region is presented in Fig. 2 as a function of depth. The errors are mostly below 3 % and does not exceed 6 %. This suggests an adequate choice of the source water types and the layer limits (Karstensen and Tomczak, 1997). The maximum errors are concentrated at the transition between the sets of source water types of layers 1 and 2, where a number of different source water types, affecting a water parcel, often exceeds the limit of 5 (see Eq. 1).

In the sensitivity test, the OMP analysis is repeated for the same sets of source water types, characteristics of which vary within some predefined limits. These limits are taken equal to the SD between the source water type characteristics, presented in different regional studies: ±0.2 °C in temperature, ±0.05 in salinity, ±20 µmol L^{-1} in oxygen, ±0.1 µmol L^{-1} in phosphates, ±1.5 µmol L^{-1} in nitrates and ±2.0 µmol L^{-1} in silicates (Karstensen and Tomczak, 1997; Pérez et al., 1998, 2001; Poole and Tomczak, 1999; van Aken, 2000a, b, 2001; Cabeçadas et al., 2002; Álvarez et al., 2004; Barbero et al., 2010; Louarn and Morin, 2011; Carracedo et al., 2014).

The sensitivity analysis reveals that the LSW and the $NADW_u$ may inter-exchange significant fractions of their percentages, when variations of source water type characteristics are close to the limiting values above. At some depths, this also occurs for different fractions of the NACW. On the other hand, the sums of the percentages of the source water types vary within 10 %, which is comparable to the variations in the resulting concentrations the mid-depths source water types (Table 2). Therefore, for further analysis we consider the sum of the percentages of the LSW and the $NADW_u$ – the North Atlantic Deep Water (NADW). For the same reason, the resulting concentrations of the StrMW, the $NACW_u$, the H and the $NACW_l$ are merged to the North Atlantic Central Water (NACW).

The sensitivity errors, averaged over the study area, together with the respective SDs are presented in Table 2. The errors are mostly under 10 %, while the MW error is below 3 %.

Summarizing the results above, 10 % contents of a source water type is taken as the error of the OMP analysis.

OSD
12, 769–822, 2015

3 Results

3.1 Distribution of source water types in the subtropical NE Atlantic

The NACW contents (Fig. 3) decreases from its maximum (90–100 %) at the upper boundary of layer 1 to 60–100 % at 700–800 m (Fig. 3a and b) and to 10–20 % already at 900–1200 m (Fig. 3c and d). The isolines of equal percentage of the NACW are mostly aligned along the neutral density surfaces, suggesting along-isopycnal spreading (Fig. 3c and d). A significant cross-isopycnal deepening of the lower boundary occurs near the Iberian Peninsula (Fig. 3c). The downwards cross-isopycnal flux is a result of the NACW entrainment by the Mediterranean Undercurrent in its rapid descend along the northern slope in the Gulf of Cadiz (Baringer and Price, 1997; Barbosa Aguiar et al., 2014), as well as of a diapycnal mixing in the Gulf of Cadiz. This deep portion of the NACW spreads southwards from the Iberian Peninsula together with the deep fraction of the MW (see below Fig. 6b).

The SAIW maximum of 45–50 % is observed in the northwestern part in the study region at 800–900 m, from where 2 maxima extend south along the both sides of the MAR (Fig. 4a and b). East of the MAR the SIAW penetrates as far south as 32° N and as far east as the Iberian Peninsula, gradually deepening to 1000 and 1200 m (Fig. 4a–d). The latter may be due to the SAIW advection by weak mid-depth eastwards flows (Iorga and Lozier, 1999a, b). The SAIW core is found between the neutral density surfaces 27.65 and 27.80 $kg\,m^{-3}$ (Fig. 4c and d). It deepens southeast with the isopycnals, but there also exists a diapycnal flux of about 0.1 $kg\,m^{-3}$ over 1000 km distance. The SAIW core becomes denser as the SAIW concentration decreases, which may be a result of mixing of the SAIW with the denser MW.

The MW contents reaches its maximum of 65 % at 1200 m at the southern margin of the Iberian Peninsula (Fig. 5a). Consistent with the pervious studies (Daniault et al., 1994; Bashmachnikov et al., 2015a), the MW maximum gets shallower northwards along the Iberian slope. Seawards, the MW reaches the highest concentration between 34 and 40° N, gradually decreasing from 60–50 to 10 % over the MAR (Figs. 5 and 6).

OSD
12, 769–822, 2015

To the south the MW makes a rather sharp front with the mAAIW at the latitude of the Canary Islands, although some traces of the MW can be detected to 25° N. The MW thickness decreases to the west (Fig. 5c): from about 1000 m near the Iberian margin and the Gulf of Caidz (between the neutral density surfaces 27.35 and 27.94 kg m^{-3}) to 100–200 m near the MAR (between 27.50 and 27.87 kg m^{-3}).

Away from the Iberian margin, the MW core deepens from 900–1000 m in the northwest to 1200–1300 m in the south and the southeast (Fig. 5b). The inclination of the isopycnals does not fully explain the depth variation. The MW maximum core is found to follow 3 different neutral density surfaces (27.70, 27.75 and 27.80 kg m^{-3}), the transitions between which occur in a jump (Figs. 5c, d and 6c, d). The positions of those jumps are schematically presented in Fig. 5b, and the areas between the density jumps represent 3 MW cores: the upper, the main and the lower cores (as compared with the previously detected 2 MW cores in Harvey and Arhan, 1988). The cores may originate at different parts of the Iberian continental slope (Fig. 5b and d) and follow different flow patterns, depending on their depth. Thus, Fig. 6a and b shows that at 800 m the MW predominantly spreads west, while at 1500 m it preferably spreads south-southwest.

The mAAIW contents maximum of around 65 % is observed in the southernmost part of the study region at about 1000 m depth (Fig. 7). The mAAIW is observed in a significant concentration (over 25 %) only south of the Canary Islands (Fig. 7a), although its northernmost limit exceeds the known one of 26–32° N (Tsuchiya et al., 1992; Alvaréz et al., 2004). As the mAAIW forms a sharp front with the MW, only deeper fractions of the mAAIW (below 1200 m) penetrate north. The core of the mAAIW deepens from 1000 (27.65 kg m^{-3}) to 1500 m (27.80 kg m^{-3}) as it progresses from 27 to 32° N, contrarily to the isopycnal slope (Fig. 7b and c). Somewhat higher mAAIW concentration at about 1000–1200 m extends north to 30–31° N only west of the Canary Islands and along the African slope.

A portion of the mAAIW enters the study region from the northwest, with the North Atlantic Current (Fig. 7a–d, see also Tsuchiya et al., 1992) at about 900 m at a low concentration of around 20 %. It spreads southeast along the eastern slope of the MAR

OSD
12, 769–822, 2015

at the lower limit of the SAIW, following the neutral density surfaces 27.55–27.80 kg m^{-3} (Fig. 7c and d). The similar paths of the mAAIW (Fig. 7a) and the SAIW (Fig. 4a) and the maximum southwards penetration of the both source water types between 20 and 25° W suggest a southwards water transport in this area.

Figure 8 presents the upper fraction of the sum of the LSW and the NADW$_u$. The LSW enters the study region from the northwest (Fig. 8a) and dominates the mixture above 1700 m (Talley and McCartney, 1982; van Aken, 2000a; Bower et al., 2002a, 2009). An interesting feature is the rise of the upper boundary of the LSW/NADW$_u$ mixture at 33–35° N, south of the Azores (Fig. 8b). We interpret this as the LSW transport across the MAR by the lower Azores Current. The LSW/NADW$_u$ mixture substantially deepens under the MW (Fig. 8b–d), as MW limits the LSW penetration (van Aken, 2000a).

Zonal and meridional sections, summarizing the areas of significant influence of the source water types (more than 25 %) are presented in Figs. 9 and 10. The NACW contents is observed above the neutral density surfaces 27.65–27.75 kg m^{-3} (around 900–1000 m). It becomes the dominating source water type (over 50 %) above 27.50–27.65 kg m^{-3}, around 800–900 m. The LSW/NADW$_u$ 25 % contents is observed below 27.70–27.85 kg m^{-3} and 50 % – below 27.80–27.88 kg m^{-3}.

The SAIW, spreading between 27.65–27.80 kg m^{-3}, has a significant input in the source water type mixture as far south as 32–36° N and as far east as 16° W. The mAAIW is found between 27.55–27.86 kg m^{-3} (900–1400 m) and 27.60–27.88 kg m^{-3} (800–1500 m) at the African slope and it has a significant contents in the source water type mixture up to 30–32° N. Over most of the region the MW mixes with the NACW above the neutral density surface 27.70–27.75 kg m^{-3} (around 1100–1200 m depth) and with the NADW/LSW below the isopycnals.

OSD
12, 769–822, 2015

3.2 Advective transport of source water types

Figure 11a presents the mean currents, derived from subsurface drifters, at 1100 m, where the contents of the SAIW, the mAAIW and the MW are close to maximum (Figs. 4b, 5b and 7b). The most intensive are the bottom trapped flows along the eastern slope of the MAR to the south (see also Bower et al., 2002a) and along the Iberian margin to the north (the Mediterranean Undercurrent). There can be also detected deep traces of the eastwards directed North Atlantic Current at 45° N and the Azores Current at 35° N. Luck of a sufficient number of observations does not permit to outline a continuous northwards bottom trapped transport along the northwestern slope of Africa, which is rather weak and intermittent (Machín and Pelegrí, 2009). The bottom trapped flow along the eastern slope of the Azores plateau and the Azores Current form a part of a large cyclonic gyre detected at 15–25° W and 34–39° N. Other features are: a westwards directed weaker flow northwest of the Iberian Peninsula, at 45° N (first detected in Bower et al., 2002a), radial spreading of water from the southwestern part of the Iberian Peninsula between 34 and 39° N, and a continuous westwards flow southwest of the Canary Islands, between 25 and 27° N. Many of the features above also exist at 1500 m level (Fig. 11c). The pathways of the MW and the mAAIW, derived from tracing the maximum percentages of their cores (Figs. 4a, 5a and 7a), are shown for selected depth levels in Fig. 11b and d. Those generally follow the major mid-depth advection patterns (Fig. 11a and c).

Overlaying the currents on the distribution of the SIAW, cut by the 1100 m section (Fig. 11a), suggests that advection along the eastern flank of the MAR and across the cyclonic gyre at 15–25° W and 34–39° N should play an important role in the southwards penetration of the SAIW the northern fraction of the mAAIW below. Further southwards penetration of the SAIW is restricted by the Azores Current.

The mAAIW principally enters in the study region along the African continental margin (Machín and Pelegrí, 2009). The flow is not seen in Fig. 11a due to luck of float data in the area, but can be clearly traced from the variation of the mAAIW concen-

OSD
12, 769–822, 2015

tration, derived with the OMP analysis (Fig. 11b). Most of the mAAIW re-circulates in the cyclonic gyre south of the Canaries and is further advected west by a zonal flow (Fig. 11a). The northernmost penetration of the mAAIW west of the Canaries does not seems to be governed by a direct northwards advection (as is seems from Fig. 11b), but by an anticyclonic circulation pattern west of the Canary Islands, centered around 20–21° W and 28–29° N (Fig. 11a). The similar pattern has been traced in the inverse model study by Carracedo et al. (2014).

Many features of the MW spreading pattern can be also related to advection (Fig. 11a and c). In particular, the MW contents over 50 % (east of 16° W) corresponds to the area of the radial water spreading from the southern and southwestern margins of the Iberian Peninsula (Fig. 11a). A weaker westwards flow north of 39° N and the cyclonic gyre between 15–25° W and 34–39° N apparently gives origin for further westwards spreading of the MW, whereas the eastwards Azores Current limits the MW spreading at the south (Fig. 11a). At 1500 m depth the radial MW spreading from the Gulf of Cadiz is limited at the west by a southwards flow parallel to the Iberian margin (Fig. 11c).

The paths, tracing the MW maximum percentage, at nearly all levels leaves the Iberian margin between Cape St. Vincent and Estremadura Promontory (Fig. 11d). The only exception is the MW path at 1800 m, which starts its southwest travel from the central Gulf of Cadiz. The deeper is the level, the farther southwards passes the corresponding path.

To better understand the role of advection/diffusion fluxes in spreading of the mid-depth source water types, currents are interpolated to local depths of the cores of the source water types (Fig. 12). The current vectors (V) are further decomposed into along-isoline ($v_{//}$) and cross-isoline ($v_{\perp}$) components, relative to the isolines of the source water type concentration (Figs. 4a, b, 5a, b and 7a, b). Further we assume that climatic distributions of the source water type concentrations are determined by a local balance between advection and turbulent diffusion: in particular, the turbulent flux of the source water type concentration should balance the cross-isoline component of

OSD
12, 769–822, 2015

the flow (Zika et al., 2010):

$$v_{\perp}\frac{\partial C}{\partial n} = \left[K_l\frac{\partial^2 C}{\partial n^2} + K_z\frac{\partial^2 C}{\partial z^2}\right] = F_{\text{diff}} \quad (2)$$

Here C is the source water type concentration, n is a normal to the isoline of C, K_l and K_z are the coefficients of horizontal and vertical diffusivity, respectively.

In Fig. 12 the magenta vectors show the areas, where advection spreads the source water type away from the source, i.e. where $v_{\perp}$ is directed along the local gradient of the source water type concentration and $v_{\perp} > v_{\text{err}}$. The error in determination of the current velocity (v_{err}) is defined in Sect. 2.1. The ratio of $v_{\perp}$ to the overall current velocity $V = \sqrt{v_{\perp}^2 + v_{//}^2}$ gives an idea of the relative importance of diffusion to advection.

The most intensive westwards advective transport of the main MW core is along 39° N, which corresponds to the direction of spreading of the main MW core, and the southwestwards advection of the lower MW core from the Gulf of Cadiz (Fig. 12a). The flows are mostly directed across isolines of the MW concentration, suggesting an intensive turbulent mixing of the MW with the surrounding water. (Fig. 12a): light color over most of the area means that turbulent diffusion largely balances the advection.

Using the gradients of the source water type concentrations, the overall turbulent diffusion fluxes (F_{diff}) are evaluated (Fig. 12b). The MW diffusion is especially strong, where the source water type spreads against the mean flow (blue arrows in Fig. 12): in a cyclonic re-circulation southwest of the Galicia Bank, at the northeastern tip of the Azores plateau and in the lower Azores Current at 34–35° N and 26–17° W. The latter two occasions are the regions of comparatively intensive jet flows, where stronger turbulent fluxes are anticipated. Those areas are also known as the areas of meddy decay: at the seamounts of the Azores plateau (Richardson et al., 2000; Bashmachnikov et al., 2009), as well as in the lateral shear of the Azores Current (Maximenko and Orlov, 1991; Bashmachnikov et al., 2015b). The backwards advection of salt from destroyed meddies may be an additional source that compensates the against-gradient advection.

OSD
12, 769–822, 2015

The mAAIW (Fig. 12c) is mostly advected along isolines of its concentration. The SAIW (Fig. 12d), as it penetrates south along the MAR, strongly mixes with the surrounding water. Since at those latitudes the SAIW penetrates into the MW core (Figs. 9 and 10), we may speculate that the horizontal mixing with the MW should be important.

Figure 11d gives evidence that the MW separates from the Iberian margin mostly between Cape St. Vincent and Estremadura Promontory (see also Daniault et al., 1994; Iorga and Lozier, 1999a). This part of the Iberian continental slope is also known to be the region of the most intensive meddy generation/detachment from the slope (Daniault et al., 1994; Bower et al., 2002b; Bashmachnikov et al., 2015b). We suggest that this is due to a local decrease of the topographic β-effect relative to the planetary β-effect in this area.

Vertically integrated geostrophic relations, together with the continuity equation, results in a well-known expression (Pedlosky, 1998):

$$\frac{v\beta}{f} - \frac{\boldsymbol{V}\cdot\nabla H}{H} = 0 \tag{3}$$

Here β is variation of the Coriolis parameter with latitude, H is the water depth, ∇H is the water depth gradient, V, as before, is the modulus of the current velocity and $v = V\cos\gamma$ is its northern component, γ is the angle between the geographic north and the direction of the flow. In the absence of external sources or sinks of relative vorticity, Eq. (3) imposes strict limitations on the direction of a geostrophic flow. When a current does not reach the bottom, only the first term (planetary β-effect) is different from zero and a geostrophic flow goes zonal ($v = 0$). When the flow reaches the bottom and the bottom slope is steep enough, the second term (topographic β-effect) becomes dominating, and a geostrophic flow follows the isobaths ($\boldsymbol{V}\cdot\nabla H = 0$). Since the MUC is known to follow the Iberian continental slope, we replace the scalar product $\boldsymbol{V}\cdot\nabla H$ with $|V|\nabla H$ and Eq. (3) becomes:

$$V\left(\frac{\beta}{f}\cos\gamma - \frac{\nabla H}{H}\right) = 0 \tag{4}$$

OSD
12, 769–822, 2015

From Eq. (4), the ratio of topographic to planetary β-effects can be written as:

$$R_\beta = \frac{\frac{\nabla H}{H}}{\frac{\beta}{f}\cos\gamma} \quad (5)$$

The bigger is R_β, the stronger is the bottom trapping of the MUC, the more difficult it is for the MUC to detach from the Iberian margin under the same intensity of the external forcing.

Figure 13a presents spatial distribution of R_β for water depth above 2000 m. Since the depth limits of the MUC are 500/600 and 1400/1500 m (Ambar and Howe, 1979; Baringer and Price, 1997; Bashmachnikov et al., 2015a), we averaged the values of R_β between 500 and 1500 m. The results are presented as a function of distance (latitude) along the 1000 m isobath, following continental slopes of the Iberian Peninsula from the southern boundary of the panel (Fig. 13a and b). There are 2 areas of particularly low R_β: one – along the southern slope of the Iberian Peninsula southeast of Faro and another one – between Cape St. Vincente and Estremadura Promontory. In the fist case, there are still two local increases of R_β across the slope: along 400–500 m isobaths and along 800–1200 m isobaths (Fig. 13a). The upper and the lower cores of the MUC follow exactly those local increase of R_β, split in the area in 2 horizontally separated veins (Ambar et al., 2008). Besides, the isolines of potential vorticity, formed by the topographic β-effect, are nearly zonal in this area, aligned with those formed by the planetary β-effect. Therefore, even if detached from the bottom slope, the MUC continues in the zonal direction and is likely to be re-trapped by the Iberian continental slope at a strong increase of R_β further west, near Cape St. Vincent. The second deepest minimum of R_β is found between Cape St. Vincente and Estremadura Promontory. Contrary to the previous case, the potential vorticity contours, formed by the topographic β-effect, are perpendicular to those formed by the planetary β-effect. Therefore, a destabilization of the MUC leads to a seawards zonal flux of the MW. Additionally, the model by Aiki and Yamagata (2004) shows that, in the absence of external forcing, meddies, after being generated from the MUC, are propagating along the con-

OSD
12, 769–822, 2015

tinental slope, trapped by topography. Decrease of the topographic β-effect north of Cape St. Vincente facilitates meddy detachment from the continental slope, which is often observed in the area (Richardson et al., 2000; Bashmachnikov et al., 2015b).

4 Discussion and conclusions

This study presents the systematic quantitative estimate of climatological distribution of the mid-depth source water type contents (the source water type volume in a unit volume of water) in the NE Atlatnic. It continues the similar studies for the NW Atlantic (Hinrichsen and Tomczak, 1993) and the NACW content in the North Atlantic (Poole and Tomczak, 1999), qualitative analysis of water mass distribution in the region (van Aken, 2000a, b, 2001), as well as analyses of particular synoptic sections (Pérez et al., 1998, 2001; Cabeçadas et al., 2002; Alvaréz et al., 2004; Barbero et al., 2010; Louarn and Morin, 2011).

Absolute values of source water type contents in each of the points depend on the choice of the source water type characteristics, different in different papers. At the same time, spatial variation of the source water type contents is much less sensible to this choice.

The results of the analysis are used to outline the spatial distributions of the depths of the source water type cores (Figs. 4–7). The variations of the core depths are found to go together with the corresponding variations of the depths of neutral density surfaces. This predominant along-isopycnal spreading of the cores presents an independent argument for the robustness of the analysis. Another argument is that directions of the main source water type pathways at different depth levels, derived from examination of the results of the OMP analysis, correspond to the advections patterns, derived from independent drifter data-sets.

The derived distributions of the mid-depth source water types do not contradict the previous studies, described in Introduction. New features and additional details are described below.

OSD
12, 769–822, 2015

4.1 The MW

In the Atlantic, away from the Iberian margin, the MW spreading has been previously separated into 2 cores (Harvey and Arhan, 1988): with the maximum at 800–1000 m (between 30 and 40° N) and with the maximum at 1500–1900 m (between 28 and 30° N). Our results suggest that 3 MW cores can be detected, separated by continuous lines of sharp gradients of the core depths/densities (Figs. 5b).

The upper MW core is found between the MAR and the transition line 28° W, 35° N – 14° W, 44° N (Fig. 5b). The MW maximum percentage lies in the neutral density range of 27.65–27.70 kg m^{-3} (900–1000 m). This corresponds to the neutral density of the maximum MW concentration at the northwestern tip of the Iberian Peninsula (Fig. 5d) or further north (Iorga and Lozier, 1999a). From the Iberian Peninsula the MW can be transported by a westwards current and farther by a southwestwards flow along the MAR (Figs. 11a and 12a, b). The maximum MW contents in the core is rather low – 10 to 25 % (Figs. 5a and 11a).

The main MW core extends from the abovementioned transition between 28° W, 35° N and 14° W, 44° N to the second transition between 35° W, 28° N and 10° W, 37° N (Fig. 5b). The first transition details the boundary between the main MW core and the SAIW/LSW (van Aken, 2000b). The MW maximum percentage in the core has neutral density around 27.75 kg m^{-3} and is observed at 1000–1100 m (Figs. 5 and 6). The neutral density of the MW core is the same as that of the MUC along the most of the western Iberian slope (Fig. 5d), but it primarily originates from the MUC between Cape St. Vincent and Estremadura Promontory (Fig. 11d) due to local decrease of the topographic β-effect (Fig. 13). The main MW core contains the most of the MW water in the Atlantic. Figure 12a and b suggests that a westwards deep flow between 38 and 40° N plays an important role in the westwards transport of the MW core. The possible role of advection in spreading of the main MW core north of 36° N has been suggested by Sparrow et al. (2002). Meanwhile the currents at mid-depths in this region are weak, of order of the first cm s^{-1}, and may be intermittent (Barbero et al., 2010). Transport by

OSD
12, 769–822, 2015

meddies is another possible mechanism, but their relative role in the westwards MW spreading is still unclear (Richardson et al., 2000; Bashmachnikov et al., 2015b).

The lower MW core, southeast of the second transition (Figs. 5b), extends from the Gulf of Cadiz southwestwards. The MW maximum percentage in the core has neutral density around 27.80 $kg\,m^{-3}$ and is observed at 1250–1350 m. The density exceeds that of the MUC even at the southern slope of the Iberian Peninsula (27.75–27.77 $kg\,m^{-3}$). The similar density in the vicinity of the Iberian Peninsula is observed only in the Gulf of Cadiz (27.79–27.80 $kg\,m^{-3}$). Here the MW influence also reaches its maximum depth of 1800–1900 m (Fig. 5d). Trapping of the MW in the cyclonic circulation of the Gulf of Cadiz (some traces of the cyclonic gyre can be seen in Fig. 11a and c), together with the anomalously low stratification of its deep waters (Iorga and Lozier, 1999a), apparently favors the MW vertical diffusion/double-diffusion to the deeper layers. The deep MW from the Gulf of Cadis is preferably advected southwest, parallel to the African margin (Fig. 12a and b). The lower MW core spreads farther west forming the boundary with the mAAIW transition at 26–29° N (Figs. 5b and 6c, d).

The MW is known to mix with both, the NACW and the NADW (Price et al., 1993; van Aken, 2000b; Barbosa Aguiar et al., 2014). Our results shows that the vertical boundary between the MW mixture with the NACW and the MW mixture with the NADW/LSW passes between the neutral density surface 27.70–27.75 $kg\,m^{-3}$, at around 1100–1200 m depth (Figs. 9 and 10).

The MW maximum contents in the MUC is around 65 %. It stays nearly constant along the Iberian margin up to 40–41° N, immediately north of Estremadura Promontory, gradually decreasing further north (see also Daniault et al., 1994). The relatively low percentage of the MW in the area of the definition of the source water type parameters (the lower core of the MUC at 7° W) is a result of artificially dilution of the MW contents in the MUC in the MEDTRANS (and other data-sets) due to the narrowness of the MUC (50 km or less) in the area. The MEDTRANS data-set fairly well represents the MW salinity in the MUC only downstream of 8–9° W (between Portimao Canyon and Cape St. Vincent), where the width of the MUC reaches 80 km and is comparable to

OSD
12, 769–822, 2015

the data-set gridding radius (Bashmachnikov et al., 2015a). Meanwhile, between 7 and 9° W the MUC transport increases by 25 % due to entrainment of the NACW/NADW (Rhein and Hinrichsen, 1993). The MW dilution to the 75 % of its contents at 7° W is expected. This is close to the estimate obtained by the OMP analysis within the 10 % error.

4.2 The SAIW

The SAIW area of influence has not been thoroughly studied in literature. Our study confirms the SAIW spreading along both sides of the MAR and nearly reaches the Iberian Peninsula to the east (McCartney and Talley, 1982; Harvey and Arhan, 1988; Arhan, 1990). At the same time, our study suggests that, east of the MAR, the SAIW spreading is not limited by 40° N (McCartney and Talley, 1982; Harvey and Arhan, 1988; Arhan, 1990), but considerable concentration of the SAIW penetrates between 20 and 25° W as far south as the Azores Current, spread over in the cyclonic gyre at 15–25° W and 34–39° N. The substantially diluted SAIW has not been reported that far south due to difficulty of differentiation of the SAIW-MW mixture from the MW mixture with the NACW or with the LSW/NADW, using traditional methods of visual inspection.

In fact, neutral density of the SAIW core (27.70–27.75 $kg\,m^{-3}$) is in the range of the neutral densities of the upper and the main MW cores (Figs. 9 and 10). The mixture between the MW and the SAIW most probably occurs as the upper/main MW cores are advected southwestwards from 42–44° N to the northeastern slope of the Azores plateau.

4.3 The mAAIW

The results of this study confirm that the overall northern limit of the mAAIW is situated between 25 and 32° N, (Tsuchiya, 1989; Tsuchiya et al., 1992; Pérez et al., 2001; Llinas et al., 2002; Alvaréez et al., 2005; Machín et al., 2006). South of 29° N the mAAIW core is positioned between the neutral density surfaces of 27.60–27.65 $kg\,m^{-3}$, at around

OSD
12, 769–822, 2015

900–1000 m. North of 29° N the mAAIW contents sharply drops down (substituted by the MW) and its core is found already between 27.80–27.85 kg m^{-3}, at 1200–1300 m. The deepening is the most drastic across the Canary Islands, which presents a natural barrier for the mAAIW spreading north. The mAAIW-MW transition equally occurs as a jump west of the Canaries, both source water types being transported west by a deep flow (Figs. 7c and 12c).

Our sensitivity experiments confirm the results by Louarn and Morin (2011) that, under different definition of the source water type characteristics, some small percentage of the mAAIW (of order of 10 %) can be detected up to the Gulf of Cadiz (not shown). Individual sections show that the mAAIW transport along the African slope already at 32° N is weak and intermittent, concentrated in a narrow coastal jet only 50–30 km wide (Machin et al., 2006; Machin and Pelegrí, 2009). Meanwhile, our study suggests that the mAAIW penetrates relatively far north also west of the Canary Islands (Figs. 7a and 11b). Its anomalous northwards penetration here can be a result of the mAAIW being trapped in an anticyclonic circulation northwest of the islands (Figs. 11a–c and 12c, see also Carracedo et al., 2014).

Appendix

Comparison our results with some previous studies

Comparison of the results of this study with previous applications of the OMP analysis along individual synoptic sections in the study region with the similar definition of the source water types (Hinrichsen and Tomczak, 1993; Alvares et al., 2004; Barbero et al., 2010) shows good correspondence (Fig. A1 and Table A1). For comparison the MW concentration are derived at the level of its maximum, while the NACW and the LSW/NADW concentrations are taken close to the levels of high vertical gradients of their concentrations. The differences in percentages of the source water types at the selected depth levels are mostly within 10–20 %: of order of 5 % for the NACW at

OSD
12, 769–822, 2015

800 m depth, 10–15 % for the MW at 1000 m depth and 10–20 % for the LSW/NADW. Partly the differences result from deviations in definitions of the characteristics of the source water types, which forms stable differences in percentages between the studies. Synoptic variability also affects individual sections vs. the climatic distribution studied here. Slightly worse correspondence for the LSW/NADW with Hinrichsen and Tomczak (1993), the squares 4 and 5, is due to the very strong vertical variation of the source water type contents at 1000 m depth (Fig. 8c and d).

Acknowledgements. The authors acknowledge the MEDTRANS scientific project (PTDC/MAR/117265/2010), sponsored by the Portuguese Foundation for Science and Technology (FCT) and the MARE – Marine and Environmental Sciences Centre of the University of Lisbon (CO-Pest-OE/MAR/UI0199/2011). I. Bashmachnikov also acknowledges contract C2008-UL-CO-3 of Ciência 2008 between the Foundation for Science and Technology (FCT) and the University of Lisbon (UL).

References

Aiki, H. and Yamagata, T.: A numerical study on the successive formation of Meddy-like lenses, J. Geophys. Res., 109, C06020, doi:10.1029/2003JC001952, 2004.

Alvaréz, M., Péres, F. F., Bryden, H., and Ríos, A. F.: Physical and biogeochemical transports structure in the North Atlantic subpolar gyre, J. Geophys. Res., 109, C03027, doi:10.1029/2003JC002015, 2004.

Ambar, I. and Howe, M. R.: Observations of the Mediterranean outflow. I. Mixing in the Mediterranean outflow, Deep-Sea Res., 26, 535–554, 1979.

Ambar, I., Serra, N., Neves, F., and Ferreira, T.: Observations of the Mediterranean Undercurrent and eddies in the Gulf of Cadiz during 2001, J. Marine Syst., 71, 195–220, 2008.

Anderson, L. A. and Sarmiento, J. L.: Redfield ratios of remineralization determined by nutrient data analysis, Global Biogeochem. Cy., 8, 65–80, doi:10.1029/93GB03318, 1994.

Arhan, M.: The North Atlantic Current and Subarctic intermediate water, J. Mar. Res., 48, 109–144, 1990.

Arhan, M., de Verdière, A. C., and Mémery, L.: The eastern boundary of the subtropical North Atlantic, J. Phys. Oceanogr., 24, 1295–1316, 1994.

OSD

12, 769–822, 2015

Barbero, L., González-Dávila, M., Santana-Casiano, J. M., and Álvarez, M.: Variability of the water mass transports and fluxes in the eastern North Atlantic during 2001, J. Geophys. Res., 115, C03023, doi:10.1029/2008JC005212, 2010.
Barbosa Aguiar, A. C., Peliz, A., Neves, F., Bashmachnikov, I., and Carton, X.: Mediterranean outflow transports and entrainment estimates from observations and high resolution modeling, Prog. Oceanogr., 131, 33–45, doi:10.1016/j.pocean.2014.11.008, 2015.
Baringer, M. O. and Price, J. F.: Mixing and spreading of the Mediterranean outflow, J. Phys. Oceanogr., 27, 1654–1677, 1997.
Barnes, S. L.: A technique for maximizing details in numerical weather map analysis, J. Appl. Meteorol., 3, 396–409, 1964.
Bashmachnikov, I., Mohn, C., Pelegrí, J. L., Martins, A., Machín, F., F. Jose, F., and White, M.: Interaction of Mediterranean water eddies with Sedlo and Seine seamounts, subtropical northeast Atlantic, Deep-Sea Res. Pt. II, 56, 2593–2605, 2009.
Bashmachnikov, I., Neves, F., Nascimento, Â., Medeiros, J., Ambar, I., Dias, J., and Carton, X.: Temperature–salinity distribution in the northeastern Atlantic from ship and Argo vertical casts, Ocean Sci., 11, 215–236, doi:10.5194/os-11-215-2015, 2015a.
Bashmachnikov, I., Neves, F., Calheiros, T., and Carton, X.: Properties and pathways of Mediterranean water eddies in the Atlantic, Prog. Oceanogr., submitted, 2015b.
Bower, A. S., Le Cann, H., Rossby, T., Zenk, W., Gould, J., Speer, K., Richardson, P. L., Prater, M. D., and Zhang, H.-M.: Directly measured mid-depth circulation in the North Atlantic Ocean, Nature, 419, 603–607, 2002a.
Bower, A., Serra, N., and Ambar, I.: Structure of the Mediterranean undercurrent and Mediterranean water spreading around the southwestern Iberian Peninsula, J. Geophys. Res., 107, 3161, doi:10.1029/2001JC001007, 2002b.
Bower, A. S., Lozier, M. S., Gary, S. F., and Böning, C. W.: Interior pathways of the North Atlantic meridional overturning circulation, Nature, 459, 243–247, 2009.
Brix, H. and Gerdes, R.: North Atlantic deep water and Antarctic bottom water: their interaction and influence on the variability of the global ocean circulation, J. Geophys. Res., 108, 3022, doi:10.1029/2002JC001335, 2003.
Cabeçadas, G., Brogueira, M. J., and Gonçalves, C.: The chemistry of Mediterranean outflow and its interactions with surrounding waters, Deep-Sea Res. Pt. II, 49, 4263–4270, 2002.
Carracedo, L. I., Gilcoto, M., Mercier, H., and Pérez, F. F.: Seasonal dynamics in the Azores–Gibraltar Strait region: a climatologically-based study, Prog. Oceanogr., 122, 116–130, 2014.

OSD
12, 769–822, 2015

Cianca, A., Santana, R., Marrero, J. P., Rueda, M. J., and Llinás, O.: Modal composition of the central water in the North Atlantic subtropical gyre, Ocean Sci. Discuss., 6, 2487–2506, doi:10.5194/osd-6-2487-2009, 2009.
Dafner, E. V., Boscolo, R., and Bryden, H. L.: The N : Si : P molar ratio in the Strait of Gibraltar, Geophys. Res. Lett., 30, 1506, doi:10.1029/2002GL016274, 2003.
Daniault, N., Mazé, J. P., and Arhan, M.: Circulation and mixing of Mediterranean water west of the Iberian Peninsula, Deep-Sea Res. Pt. I, 41, 1685–1714, 1994.
Garcia, D.: A fast all-in-one method for automated post-processing of PIV data, Exp. Fluids, 50, 1247–1259, 2011.
Harvey, J. and Arhan, M.: The water masses in central North Atlantic in 1983–84, J. Phys. Oceanogr., 18, 1855–1875, 1988.
Hinrichsen, H.-H. and Tomczak, M.: Optimum multiparameter analysis of the water mass structure in the western North Atlantic Ocean, J. Geophys. Res., 98, 10155–10169, doi:10.1029/93JC00180, 1993.
Iorga, M. C. and Lozier, M. S.: Signatures of the Mediterranean outflow from a North Atlantic climatology. 1. Salinity and density fields, J. Geophys. Res., 104, 25985–26009, 1999a.
Iorga, M. C. and Lozier, M. S.: Signatures of the Mediterranean outflow from a North Atlantic climatology. 2. Diagnostic velocity fields, J. Geophys. Res., 104, 26011–26029, 1999b.
Jackett, D. R. and McDougall, T. J.: A neutral density variable for the World's oceans, J. Phys. Oceanogr., 27, 237–263, 1997.
Karstensen, J. and Tomczak, M.: Ventilation processes and water mass ages in the thermocline of the southeast Indian Ocean, Geophys. Res. Lett., 24, 2777–2780, doi:10.1029/97GL02708, 1997.
Klein, B. and Tomczak, M.: Identification of diapycnal mixing through optimum multiparameter analysis: 2. Evidence for unidirectional diapycnal mixing in the front between North and South Atlantic central water, J. Geophys. Res., 99, 25275–25280, doi:10.1029/94JC01948, 1994.
Krémeur, A.-S., Lévy, M., Aumont, O., and Reverdin, G.: Impact of the subtropical mode water biogeochemical properties on primary production in the North Atlantic: new insights from an idealized model study, J. Geophys. Res., 114, C07019, doi:10.1029/2008JC005161, 2009.
Lavender, K. L., Owens, W. B., and Davis, R. E.: The mid-depth circulation of the subpolar North Atlantic Ocean as measured by subsurface floats, Deep-Sea Res. Pt. I, 52, 767–785, doi:10.1016/j.dsr.2004.12.007, 2005.

OSD
12, 769–822, 2015

Llinás, O., Rueda, M. J., Pérez Marrero, J., Pérez-Martell, E., Santana, R., Villagarcìa, M. G., Cianca, A., Godoy, J., and Maroto, L.: Variability of the Antarctic intermediate waters in the northern Canary box, Deep-Sea Res. Pt. II, 49, 3441–3453, doi:10.1016/S0967-0645(02)00090-5, 2002.
Louarn, E. and Morin, P.: Antarctic intermediate water influence on Mediterranean sea water outflow, Deep-Sea Res. Pt. I, 58, 932–942, doi:10.1016/j.dsr.2011.05.009, 2011.
Machín, F. and Pelegrí, J. L.: Northward penetration of Antarctic intermediate water off northwest Africa, J. Phys. Oceanogr., 39, 512–535, 2009.
Machín, F., Hernández-Guerra, A., and Pelegrí, J. L.: Mass fluxes in the Canary Basin, Prog. Oceanogr., 70, 416–447, doi:10.1016/j.pocean.2006.03.019, 2006.
Mackas, D. L., Denman, K. L., and Bennett, A. F.: Least squares multiple tracer analysis of water mass composition, J. Geophys. Res., 92, 2907–2918, 1987.
Mailly, T., Blayo, E., and Verron, J.: Assessment of the ocean circulation in the Azores region as predicted by a numerical model assimilating altimeter data from Topex/Poseidon and ERS-1 satellites, Ann. Geophys., 15, 1354–1368, doi:10.1007/s00585-997-1354-x, 1997.
Maximenko, N. A. and Orlov, O. I.: Integral characteristics of the core of quasi-stationary "Gauss" vortex in homogeneous and shear flows, Oceanology, 31, 34–41, 1991 (in Russian).
Mazé, G. and Marshall, J.: Diagnosing the observed seasonal cycle of Atlantic subtropical mode water using potential vorticity and its attendant theorems, J. Phys. Oceanogr., 41, 1986–1999, 2011.
Mazé, J. P., Arhan, M., and Mercier, H.: Volume budget of the eastern boundary layer off the Iberian Peninsula, Deep-Sea Res. Pt. I, 44, 1543–1574, 1997.
McCartney, M. S.: The subtropical recirculation of mode waters, J. Mar. Res., 40, 427–464, 1982.
McCartney, M. S. and Talley, L. D.: The subpolar mode water of the North Atlantic Ocean, J. Phys. Oceanogr., 12, 1169–1188, 1982.
McDougall, T. J.: Neutral density surfaces, J. Phys. Oceanogr., 17, 1950–1964, 1987.
Morel, Y.: The influence of an upper thermocline current on intrathermocline eddies, J. Phys. Oceanogr., 25, 3247–3252, 1995.
New, A. L., Jia, Y., Coulibaly, M., and Dengg, J.: On the role of the Azores current in the ventilation of the North Atlantic Ocean, Prog. Oceanogr., 48, 163–194, 2001.

OSD
12, 769–822, 2015

Ollitrault, M. and Colin de Verdière, A.: The ocean general circulation near 1000-m depth, J. Phys. Oceanogr., 44, 384–409, 2014.
Orsi, A. H., Jacobs, S. S., Gordon, A. L., and Visbeck, M.: Cooling and ventilating the Abyssal Ocean, Geophys. Res. Lett., 28, 2923–2926, doi:10.1029/2001GL012830, 2001.
Paillet, J. and Arhan, M.: Shallow picnocline and mode water subduction in the eastern North Atlantic, J. Phys. Oceanogr., 26, 96–114, 1996a.
Paillet, J. and Arhan, M.: Oceanic ventilation in the eastern North Atlantic, J. Phys. Oceanogr., 26, 2036–2052, 1996b.
Paillet, J., Arhan, M., and McCartney, M. S.: Spreading of Labrador Sea water in the eastern North Atlantic, J. Geophys. Res., 103, 10223–10239, 1998.
Pedlosky, J.: Ocean Circulation Theory, 2nd edn., Springer, New York, 1–453, 1998.
Pérez, F. F., Mouriño, C., Fraga, F., and Rios, A. F.: Displacement of water masses and remineralization rates off the Iberian Peninsula by nutrient anomalies, J. Mar. Res., 51, 869–892, 1993.
Pérez, F. F., Ríos, A. F., Castro, C. G., and Fraga, F.: Mixing analysis of nutrients, oxygen and dissolved inorganic carbon in the upper and middle North Atlantic Ocean east of the Azores, J. Marine Syst., 16, 219–233, 1998.
Pérez, F. F., Mintrop, L., Llinás, O., Glez-Dávila, M., Castro, C. G., Alvaréz, M., Körtzinger, A., Santana-Casiano, M., Rueda, M. J., and Ríos, A. F.: Mixing analysis of nutrients, oxygen and dissolved inorganic carbon in Canary Islands region, J. Marine Syst., 28, 183–201, 2001.
Pingree, R. D., Garcia-Soto, C., and Sinha, B.: Position and structure of the subtropical/Azores front region from combined Lagrangian and remote sensing (IR/altimiter/SeaWiFS) measurements, J. Mar. Biol. Assoc. UK, 79, 769–792, 1999.
Pollard, R. T. and Pu, S.: Structure and circulation of the upper Atlantic Ocean northeast of the Azores, Prog. Oceanogr., 14, 443–462, 1985.
Pollard, R. T., Griffiths, M. J., Cunningham, S. A., Read, J. F., Pérez, F. F., and Rios, A. F.: Vivaldi 1991 – a study of the formation, circulation and ventilation of eastern North Atlantic central water, Prog. Oceanogr., 37, 167–192, 1996.
Poole, R. and Tomczak, M.: Optimum multiparameter analysis of the water mass structure in the Atlantic Ocean thermocline, Deep-Sea Res. Pt. I, 46, 1895–1921, 1999.
Price, J. F., Baringer, M., Lueck, R. G., Johnson, G. C., Ambar, I., Parrilla, G., Cantos, A., Kennelly, M. A., and Sanford, T. B.: Mediterranean outflow mixing and dynamics, Science, 259, 1277–1282, 1993.

OSD
12, 769–822, 2015

Redfield, A. C., Ketchum, B. H., and Richards, F. A.: The influence of organisms on the composition of sea-water, in: The Sea: Ideas and Observations on Progress in the Study of the Seas, vol. 2, edited by: Hill, M. N., Wiley, London, 26–77, 1963.

Rhein, M. and Hinrichsen, H.-H.: Modification of Mediterranean water in the Gulf of Cadiz, studied with hydrographic, nutrient and chlorofluoromethane data, Deep-Sea Res. Pt. I, 40, 267–291, 1993.

Richardson, P. L., McCartney, M. S., and Maillard, C.: A search for meddies in historical data, Dynam. Atmos. Oceans, 15, 241–265, 1991.

Richardson, P. L., Bower, A. S., and Zenk, W.: A census of Meddies tracked by floats, Prog. Oceanogr., 45, 209–250, 2000.

Schmitz Jr., W. J.: On the World Ocean Circulation. Volume 1. Some Global Features/North Atlantic Circulation, No. WHOI-96-03-VOL-1, Woods Hole Oceanographic Institution, Woods Hole, MA, 1996.

Siedler, G., Kuhl, A., and Zenk, W.: The Madeira mode water, J. Phys. Oceanogr., 17, 1561–1570, 1987.

Sparrow, M., Boebel, O., Zervakis, V., Zenk, W., Cantós-Figueroa, A., and Gould, W. J.: Two circulation regimes of the Mediterranean outflow revealed by Lagrangian measurements, J. Phys. Oceanogr., 32, 1322–1330, 2002.

Stramma, L., Brandt, P., Schafstall, J., Schott, F., Fischer, J., and Körtzinger, A.: Oxygen minimum zone in the North Atlantic south and east of the Cape Verde Islands, J. Geophys. Res., 113, C04014, doi:10.1029/2007JC004369, 2008.

Straneo, F., Pickart, R. S., and Lavender, K.: Spreading of Labrador Sea water: an advective-diffusive study based on Lagrangian data, Deep-Sea Res. Pt. I, 50, 7001–719, 2003.

Talley, L. D. and McCartney, M. S.: Distribution and circulation of Labrador Sea water, J. Phys. Oceanogr., 12, 1189–1205, 1982.

Tomczak, M.: A multiparameter extension of temperature/salinity diagram techniques for the analysis of non-isopycnal mixing, Prog. Oceanogr., 10, 147–171, 1981.

Tomczak, M. and Godfrey, J. S.: Regional Oceanography: an Introduction, available at: http://www.es.flinders.edu.au/~mattom/regoc/pdfversion.html (last access: 08.05.2015), 2003.

Tomczak, M. and Large, D. G.: Optimum multiparameter analysis of mixing in the thermocline of the eastern Indian Ocean, J. Geophys. Res., 94, 16141–16149, doi:10.1029/JC094iC11p16141, 1989.

OSD
12, 769–822, 2015

Tsuchiya, M.: Circulation of the Antarctic intermediate water in the North Atlantic Ocean, J. Mar. Res., 47, 747–755, 1989.
Tsuchiya, M., Talley, L. D., and McCartney, M. S.: An eastern Atlantic section from Iceland southward across the equator, Deep-Sea Res., 39, 1885–1917, 1992.
van Aken, H. M.: The hydrography of the mid-latitude northeast Atlantic Ocean I: The deep water masses, Deep-Sea Res. Pt. I, 47, 757–788, 2000a.
van Aken, H. M.: The hydrography of the mid-latitude northeast Atlantic Ocean II: The intermediate water masses, Deep-Sea Res. Pt. I, 47, 789–824, 2000b.
van Aken, H. M.: The hydrography of the mid-latitude northeast Atlantic Ocean III: The subducted thermocline water mass, Deep-Sea Res. Pt. I, 48, 237–267, 2001.
Zika, J. D., McDougall, T. J., and Sloyan, B. M.: Weak mixing in the eastern North Atlantic: an application of the Tracer-Contour Inverse Method. J. Phys. Oceanogr., 40, 1881–1893, 2010.

OSD
12, 769–822, 2015

Table 1. Source Water Type characteristics for the subtropical Mode Water (StrMW), the North Atlantic Central Water ($NACW_u$, H and $NACW_l$), the Mediterranean Water (MW), the modified Antarctic Intermediate Water (mAAIW), the Subarctic Intermediate Water (SAIW), the Labrador Sea Water (LSW), and the upper North Atlantic Deep Water ($NADW_u$).

Water type	θ (°C)	S	O_2 ($\mu mol\,L^{-1}$)	PO_4 ($\mu mol\,L^{-1}$)	NO_3 ($\mu mol\,L^{-1}$)	Si ($\mu mol\,L^{-1}$)
StrMW	19.0	36.70	100	0.16	2.0	2.0
$NACW_u$	18.0	36.45	250	0.15	2.0	2.0
H	12.2	35.60	230	0.70	12.0	4.5
$NACW_l$	8.8	35.15	195	1.20	20.0	12.0
MW	13.2	37.10	170	1.00	16.0	7.0
mAAIW	6.5	34.90	110	2.10	32.0	23.0
SAIW	5.6	34.70	280	1.00	15.0	6.0
LSW	3.4	34.89	295	1.10	17.0	12.0
$NADW_u$	2.5	34.94	250	1.30	20.0	35.0
Weight	24	22	7	2	7	1

OSD
12, 769–822, 2015

Table 2. Mean error and respective SD of the results of OMP analysis regarding the sensitivity experiments. The upper limit of the error comprises 99 % of the errors obtained in the sensitivity analysis over the whole study area.

Water type	Mean error ± SD (%)	Upper limit of the error (%)
NACW	5 ± 1	9
SAIW	9 ± 1	13
MW	2 ± 0	3
mAAIW	5 ± 1	7
LSW+$NADW_u$	6 ± 1	8

OSD
12, 769–822, 2015

Table 3. List of the main acronyms.

mAAIW	modified Antarctic Intermediate Water
AAIW	Antarctic Intermediate Water
H	North Atlantic Central Water, the maximum inflection point
LSW	Labrador Sea Water
MAR	Mid Atlantic Ridge
MW	Mediterranean Water
NACW	North Atlantic Central Water
NADW	North Atlantic Deep Water
OMP	Optimum Multiparameter
SAIW	Subarctic Intermediate Water
StrMW	subtropical Mode Water

OSD
12, 769–822, 2015

Table A1. A comparison of percentages obtained by applying the OMP analysis. The column "Lit." shows the range of percentages of a source water type in a literature source, the definitions of source water types characteristics from which are used to derive source water types characteristics for this study. The difference is computed between the mean values in a 5° × 5° square (Fig. A1) between the literature source and this work.

	Lit.	this paper (difference) NACW, 800 m	Lit.	this paper (difference) MW, 1000 m	Lit.	this paper (difference) LSW/NADW, 1000 m
1	50–60[a]	57 (−2 %)	60[a]	45 (−15 %)	30–50[a]	29 (−12 %)
2	60–80[a], 70[b]	72 (−2 %)	40–50[a], 30–50[b]	35 (−11 %)	50–60[a], 70[b]	46 (−9 %)
3	80–90[a]	76 (−9 %)	20–40[a]	25 (−5 %)	50–70[a]	62 (−2 %)
4	85[c]	78 (−8 %)	5[c]	22 (−17 %)	76[c]	54 (−23 %)
5	82[c]	73 (−9 %)	6[c]	20 (−14 %)	81[c]	61 (−20 %)

[a] Alvaréz et al. (2004).
[b] Barbero et al. (2010).
[c] Hinrichsen and Tomczak (1993).

OSD
12, 769–822, 2015

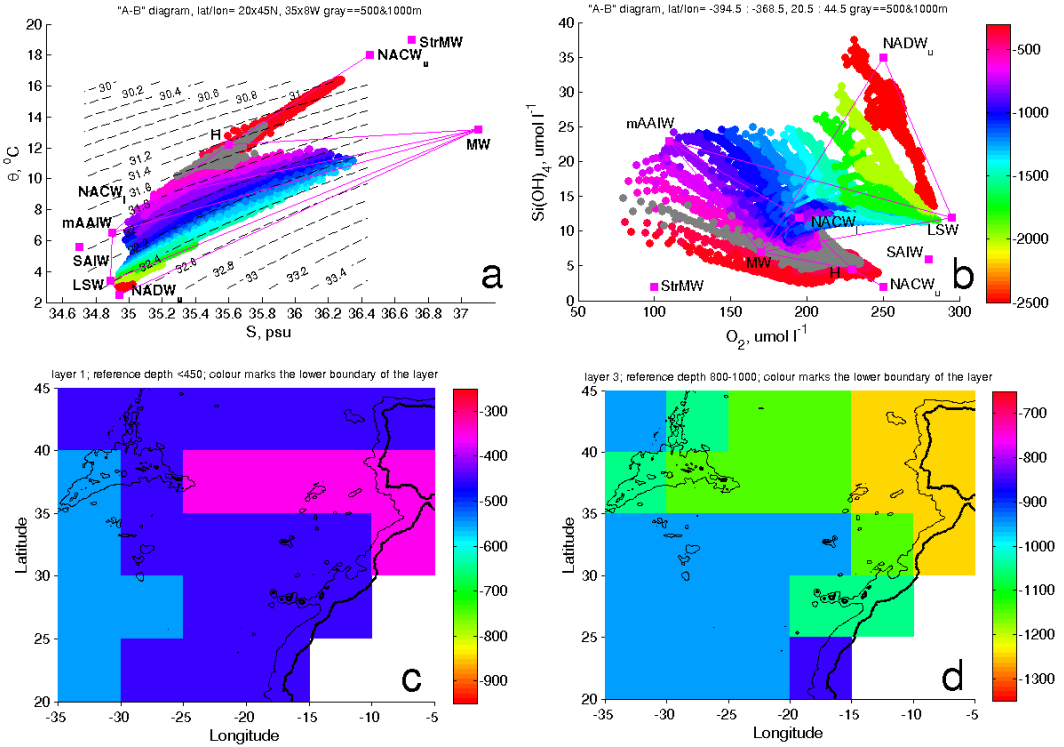

Figure 1. (a) θ-S diagram; **(b)** Si-O_2 diagram; **(c)** depth of the lower limit of layer 1 (m); **(d)** depth of the lower limit of layer 2 (m). Color scale in plates **(a)** and **(b)** presents depth of the sample. The isopycnals in plate **(a)**, referenced to 1000 m (σ_1), has illustrative value.

OSD
12, 769–822, 2015

Distribution of intermediate water masses in the subtropical northeast Atlantic

I. Bashmachnikov et al.

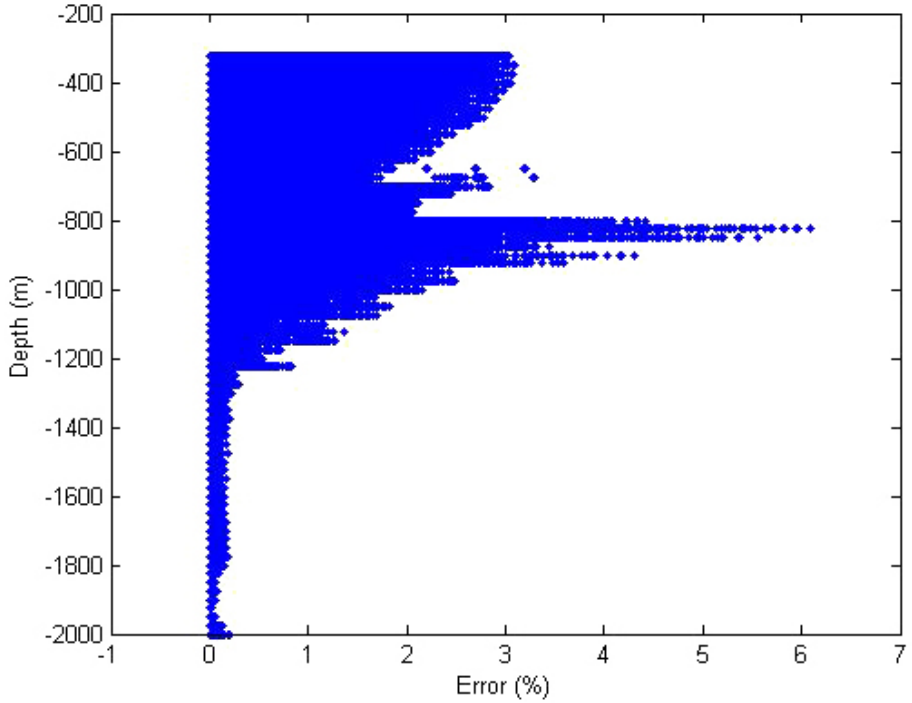

Figure 2. OMP mass conservation residuals (R_Σ). The residuals represent the difference between the theoretical value obtained with the result of the OMP analysis and the observed data.

OSD
12, 769–822, 2015

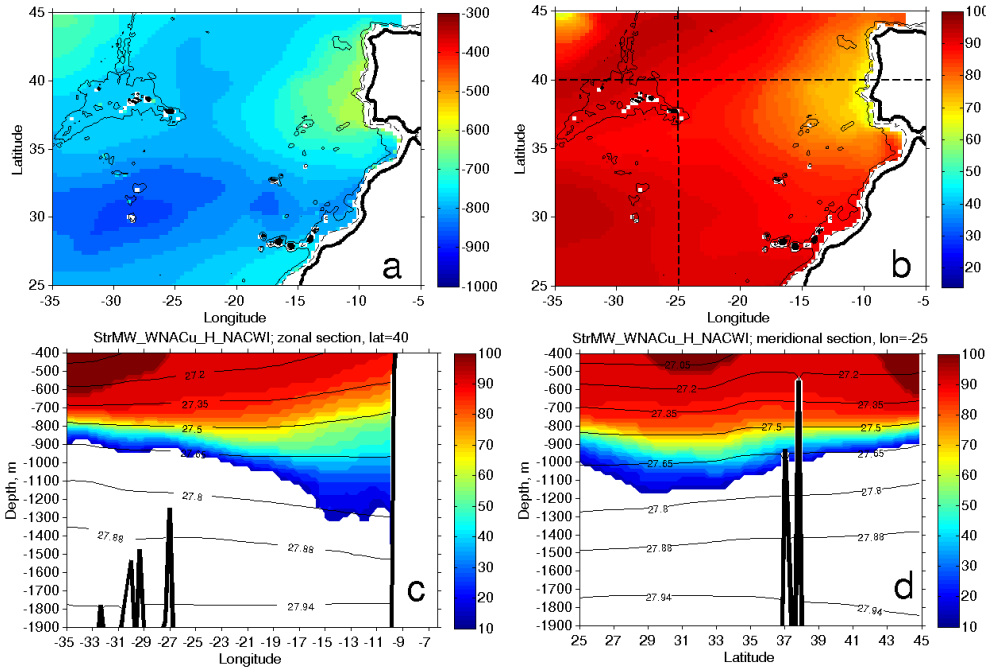

Figure 3. The NACW: **(a)** depth of 50 % of the NACW content. **(b)** NACW content (%) at 700 m. Isobaths of 500 and 2000 m are marked in dashed and solid black lines, respectively. Zonal and meridional sections, presented in plates (**c** and **d**), are marked with dashed black lines. **(c)** Zonal section of the NACW content (%) along 40° N; **(d)** meridional section of the NACW content (%) along 25° W. Solid black lines are neutral density surfaces.

OSD
12, 769–822, 2015

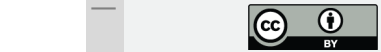

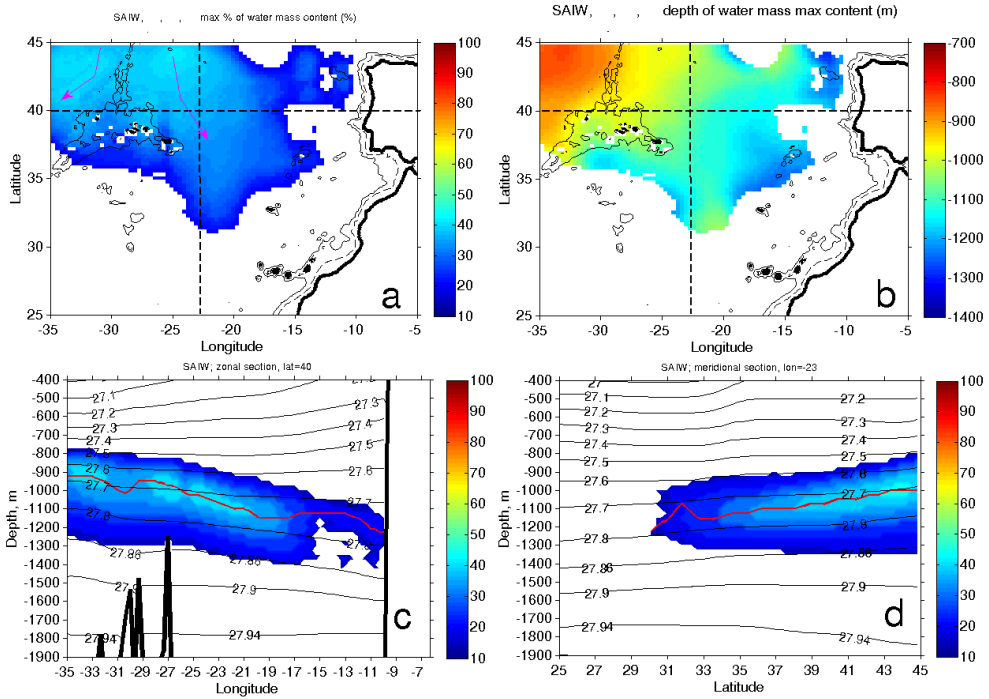

Figure 4. The SAIW: **(a)** maximum percentage in the water column, magenta lines mark suggested pathways of the SAIW; **(b)** depth (m) at which the maximum percentage in the water column is reached. Isobaths of 500 and 2000 m are marked in dashed and solid black lines, respectively. Zonal and meridional sections, presented in plates (**c** and **d**), are marked with dashed black lines. **(c)** Zonal section of the SAIW content (%) along 40° N; **(d)** meridional section of the SAIW content (%) along 23° W. Solid black lines are neutral density surfaces. Red line marks the depth of the maximum content of the source water type in the water column.

OSD
12, 769–822, 2015

Distribution of intermediate water masses in the subtropical northeast Atlantic

I. Bashmachnikov et al.

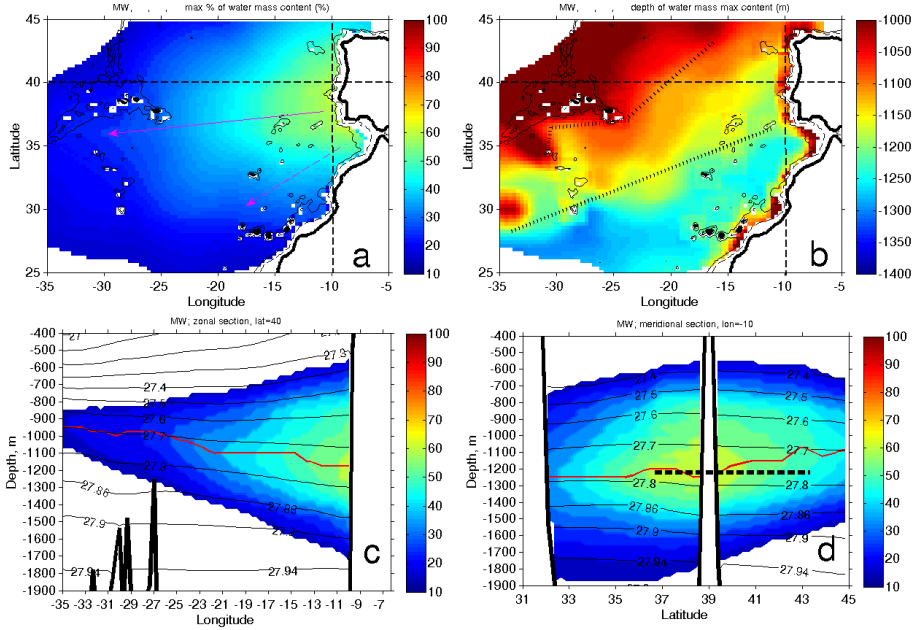

Figure 5. The MW. **(a)** Maximum percentage in the water column, magenta lines mark suggested pathways of the MW; solid line – main MW core, dashed line – lower MW core. **(b)** Depth (m) at which the maximum percentage in the water column is reached; the black dotted liens mark the maximum core-depth gradients. Isobaths of 500 and 2000 m are marked in dashed and solid black lines, respectively. Zonal and meridional sections, presented in plates (**c** and **d**), are marked with dashed black lines. **(c)** Zonal section of the MW content (%) along 40° N; **(d)** meridional section of the MW content (%) along 10° W (the topographic rise at 39° N is Estremadura Promontory). Solid black lines are neutral density surfaces. In plate **(d)** the black thick dashed line marks the limits of the meridional extension of the continental slope of the Iberian Peninsula to the east of the section. Red line marks the depth of the maximum content of the source water type in the water column.

OSD
12, 769–822, 2015

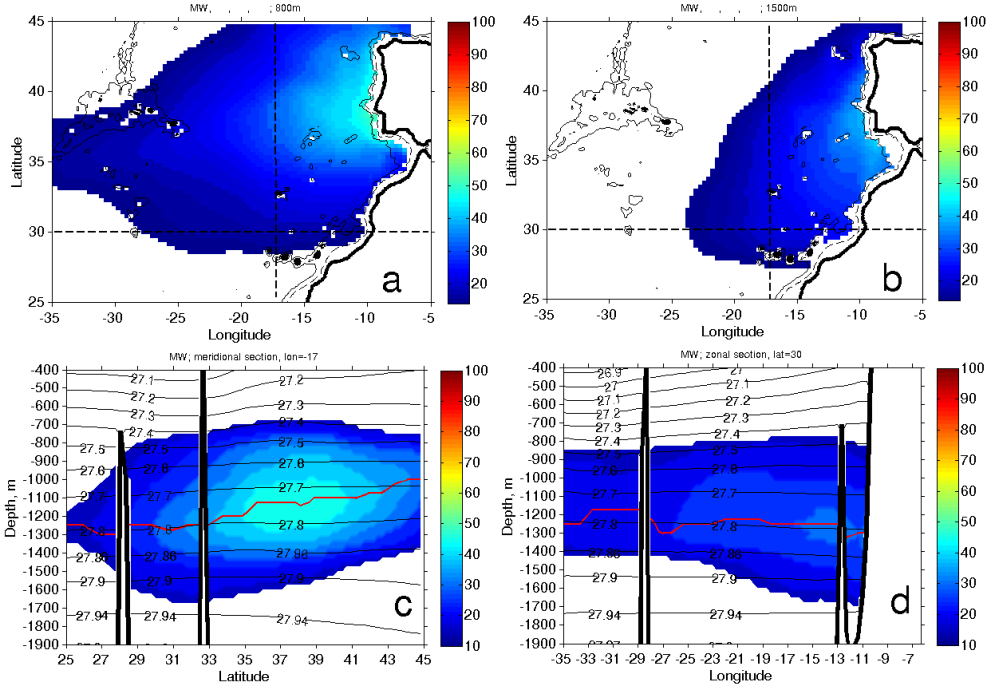

Figure 6. The MW content (%) at **(c)** 800 m and at **(d)** 1500 m depth. Isobaths of 500 and 2000 m are marked in dashed and solid black lines, respectively. Zonal and meridional sections, presented in plates (**c** and **d**), are marked with dashed black lines. **(c)** Meridional section of the MW content (%) along 17° W; **(d)** zonal section of the MW content (%) along 29° N. Solid black lines are neutral density surfaces. Red line marks the depth of the maximum content of the source water type in the water column.

OSD
12, 769–822, 2015

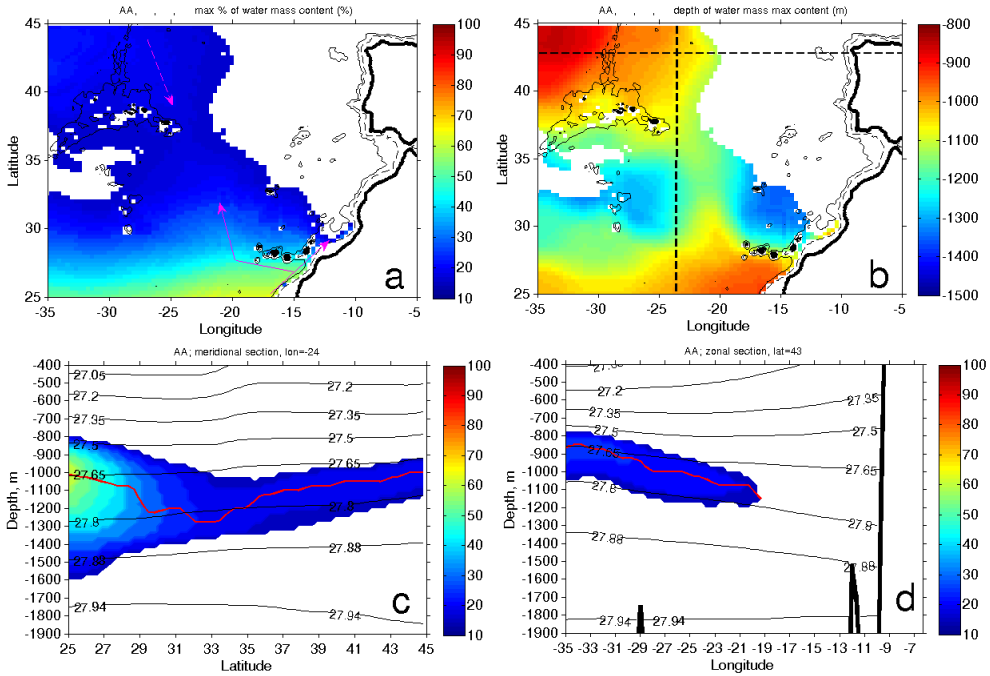

Figure 7. The mAAIW: **(a)** maximum percentage in the water column, magenta lines mark suggested pathways of the mAAIW (solid line), and modified mAAIW (dashed line); **(b)** depth (m) at which the maximum percentage in the water column is reached. Isobaths of 500 and 2000 m are marked in dashed and solid black lines, respectively. Zonal and meridional sections, presented in plates (**c** and **d**), are marked with dashed black lines. **(c)** Meridional section of the mAAIW content (%) along 24° W; **(d)** zonal section of the mAAIW content (%) along 43° N. Red line marks the depth of the maximum content of the source water type in the water column.

OSD
12, 769–822, 2015

Distribution of intermediate water masses in the subtropical northeast Atlantic

I. Bashmachnikov et al.

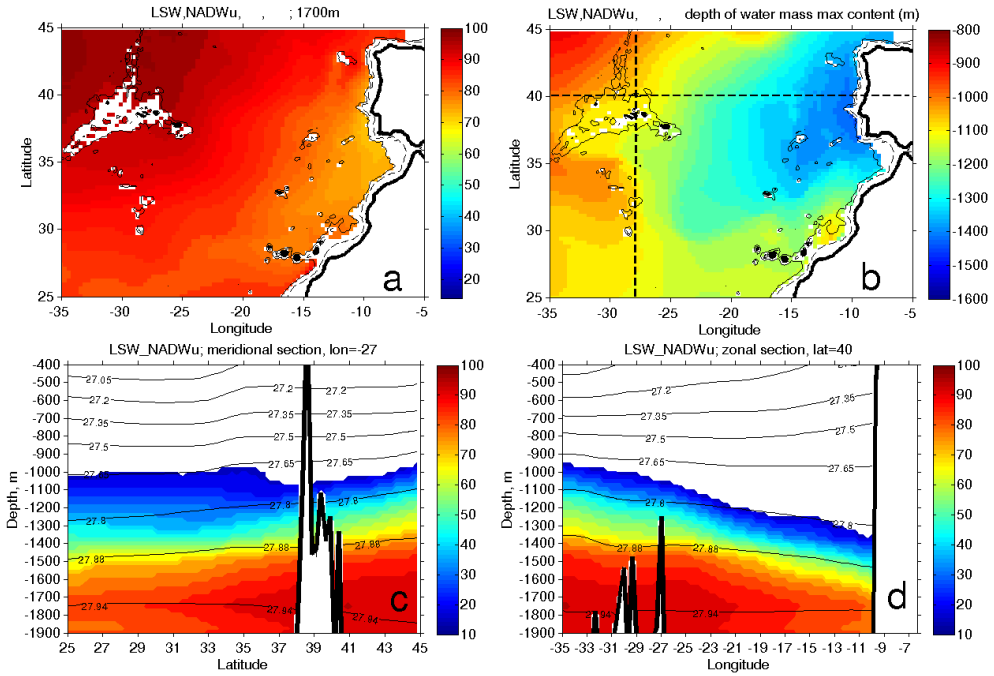

Figure 8. The LSW and the $NADW_u$ **(a)** LSW + $NADW_u$ content (%) at 1700 m. **(b)** Depth of 25 % of the LSW + $NADW_u$ content. Isobaths of 500 and 2000 m are marked in dashed and solid black lines, respectively. Zonal and meridional sections, presented in plates (**c** and **d**), are marked with dashed black lines. **(c)** Meridional section of the LSW + $NADW_u$ content (%) along 27° W; **(d)** zonal section of the LSW + $NADW_u$ content (%) along 40° N.

OSD
12, 769–822, 2015

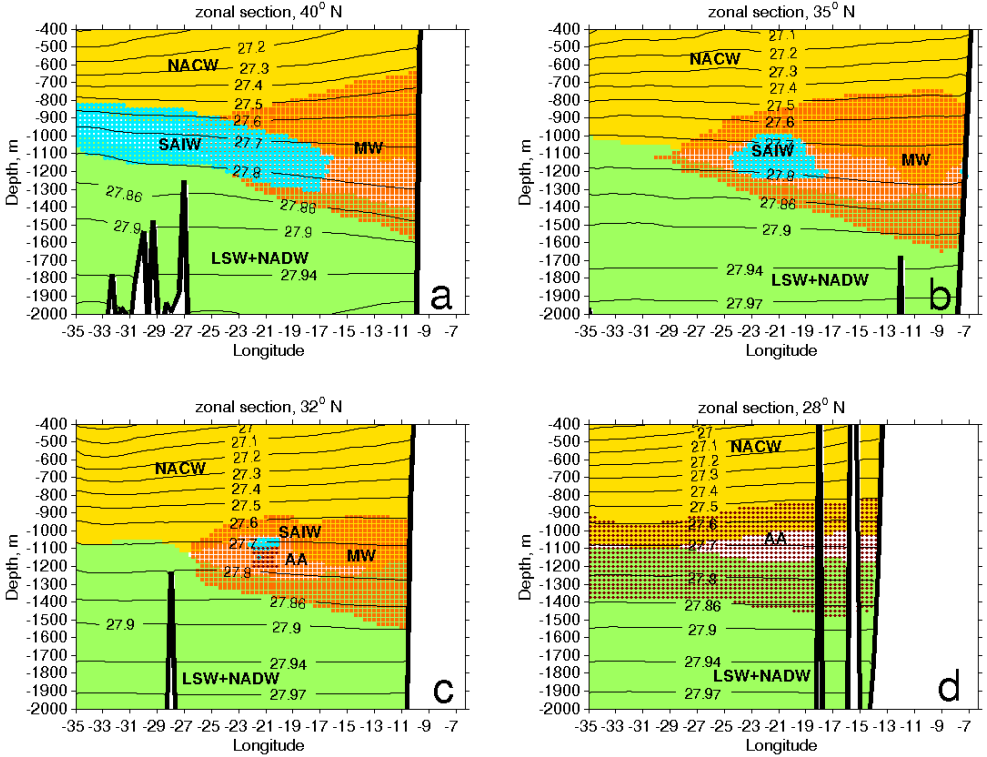

Figure 9. The dominant water masses along zonal sections **(a)** 40° N, **(b)** 35° N, **(c)** 32° N, **(d)** 28° N. Yellow is the NACW, green – the LSW and the NADW, orange – the MW, cyan – the SAIW, brown – the mAAIW, only water mass contents over 25 % are shown.

OSD
12, 769–822, 2015

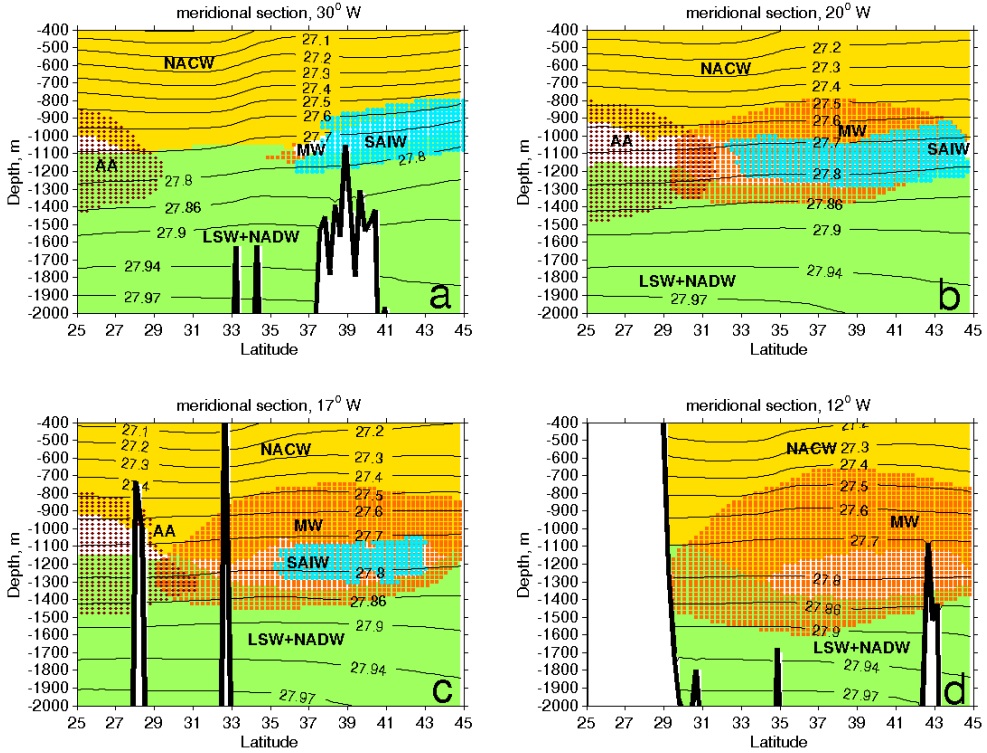

Figure 10. The dominant water masses along meridional sections **(a)** 30° W, **(b)** 20° W, **(c)** 17° W, **(d)** 12° W. Yellow is the NACW, green – the LSW and the NADW, orange – the MW, cyan – the SAIW, brown – the mAAIW, only water mass contents over 25 % are shown.

OSD
12, 769–822, 2015

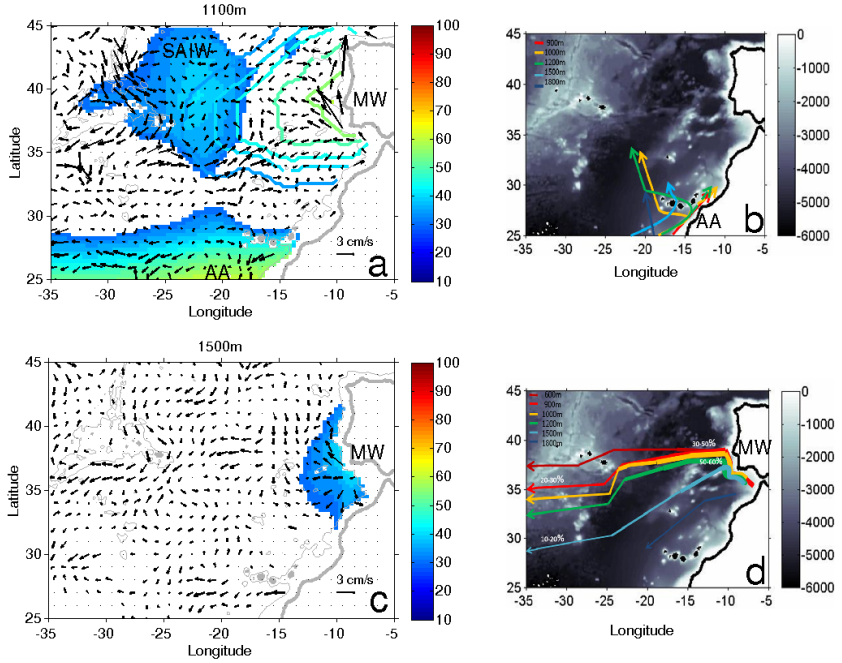

Figure 11. (a) Source water type contents (%) at 1100 m: the SAIW (northwest, color), the mAAIW (south, color) and the MW (west, contours). Only source water type concentrations over 25 % are presented. Current vectors at 1100 m depth are overlaid. **(b)** Paths of the mAAIW at different depth levels based on variation of the source water type contents. **(c)** The MW contents (%) at 1500 m (color). Only the source water type concentrations over 25 % are presented. Current vectors at 1500 m depth are overlaid. **(d)** Paths of the MW at different depth levels based on variation of the source water type contents. In plates (**b** and **d**): dark red is 600 m, red – 900 m, yellow – 1000 m, green – 1200 m, light blue – 1500 m, thin dark blue line – 1800 m. The line thickness in **(d)** demonstrate the MW contents, which varies from 30–60 % in the east to 10–20 % in the west of the region.

OSD
12, 769–822, 2015

Distribution of intermediate water masses in the subtropical northeast Atlantic

I. Bashmachnikov et al.

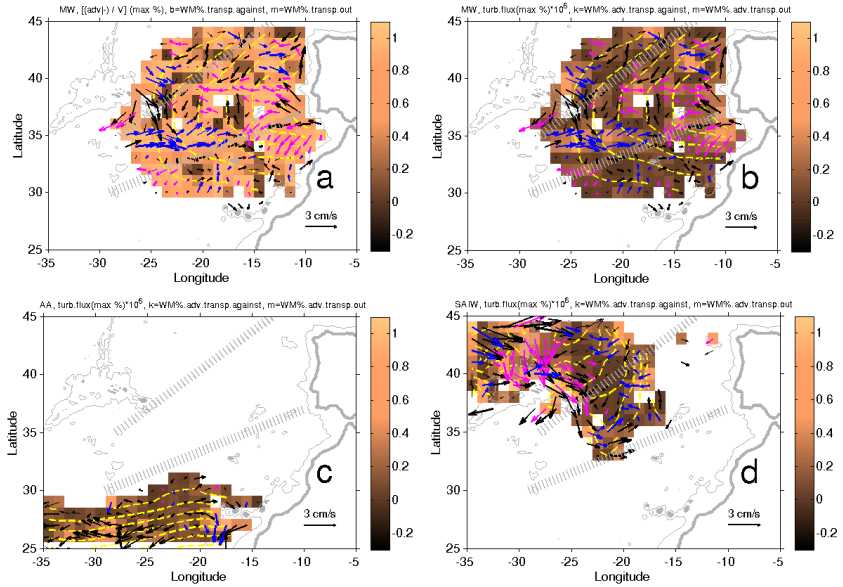

Figure 12. Relative role of advective fluxes in source water type core spreading. Color in plate **(a)** is $|v_\perp/V|$ over the MW, the lighter is the color the closer is the advection balanced by diffusive dispersion of the source water type contents. Plates **(b–d)** represent the relative intensity of the diffusive fluxes (F_{diff}) for the MW, the mAAIW and the SAIW, respectively. Currents at the core depth of the respective source water type are marked with thin black arrows (the error in definition of the current velocity ranges from 50 to 100 %) and thick black/magenta/blue arrows (the error in definition of the current velocity is below 50 %). Yellow contours represent isolines of concentrations of the respective source water type. Black arrows additionally mark the currents that advect concentrations predominantly along the isolines of the source water type concentration, magenta – away from the source water type source (from higher to lower source water type concentration), blue – towards the source (from lower to higher source water type concentration). The boundaries of the 3 MW cores are marked as dotted gray lines. Solid gray lines present the 2000 m isobath and the coastline.

OSD
12, 769–822, 2015

Distribution of intermediate water masses in the subtropical northeast Atlantic

I. Bashmachnikov et al.

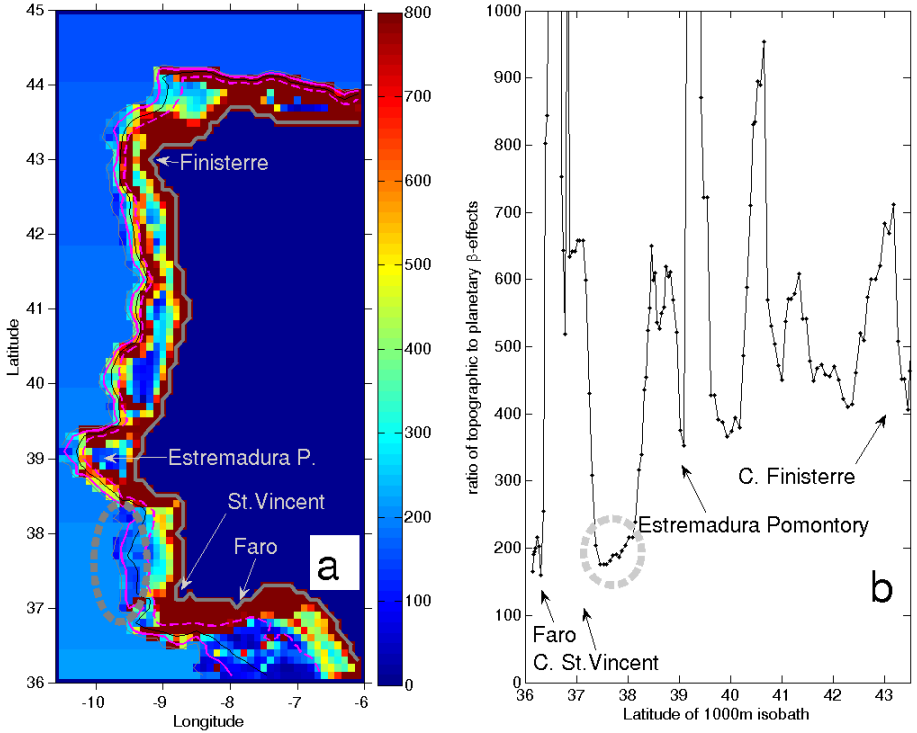

Figure 13. Ratio of topographic β-effect to planetary β-effect (R_β) for a flow, trapped by the Iberian margin. **(a)** Spatial distribution of R_β. Where water depth exceeds 2000 m only planetary β-effect is plotted; for meridional variations to be visible in the plot β/f are multiplied by 10^9. Isobaths of 500 m (white dashed line) and 1500 m (white solid line) are marked. **(b)** Mean R_β between 500 and 1500 m, x coordinate are latitudes of 1000 m isobath. In both plates the gray ellipses mark the place with the lowest R_β.

OSD
12, 769–822, 2015

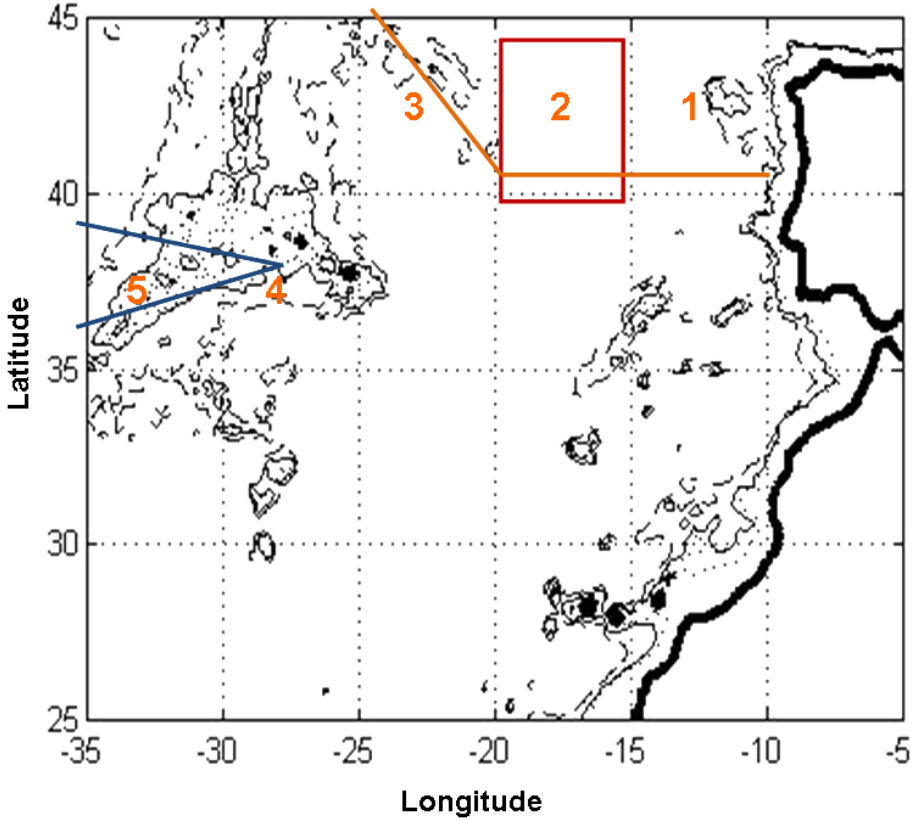

Figure A1. A map of sections along which comparison with the previous literature results in 5° × 5° squares are made: blue line – Hinrichsen and Tomczak (1993); orange line – Alvaréz et al. (2004); red square – Barbero et al. (2010). Squares, where the results are averaged are numbered.

OSD
12, 769–822, 2015